MDPI

Article

Anti-Leukemic Properties of Aplysinopsin Derivative EE-84 Alone and Combined to BH3 Mimetic A-1210477

Sungmi Song [1,†], Sua Kim [1,†], Eslam R. El-Sawy [2,3], Claudia Cerella [1,4], Barbora Orlikova-Boyer [1,4], Gilbert Kirsch [3], Christo Christov [5], Mario Dicato [4] and Marc Diederich [1,*]

1   Department of Pharmacy, College of Pharmacy, Seoul National University, 1 Gwanak-ro, Gwanak-gu, Seoul 08626, Korea; sson35@snu.ac.kr (S.S.); suakim@snu.ac.kr (S.K.); claudia.cerella@lbmcc.lu (C.C.); barbora.orlikova@lbmcc.lu (B.O.-B.)
2   Chemistry Department of Natural Compounds, National Research Centre, Dokki, 12622 Giza, Egypt; eslamelsawy@gmail.com
3   UMR CNRS 7565 SRSMC, Université du Lorraine, 57070 Metz, France; gilbert.kirsch@univ-lorraine.fr
4   Laboratoire de Biologie Moléculaire et Cellulaire du Cancer, Hôpital Kirchberg, 9, Rue Edward Steichen, 2540 Luxembourg, Luxembourg; dicato.mario@chl.lu
5   Service d'Histologie, Faculté de Médicine, Université de Lorraine, INSERM U1256 NGERE, 54000 Nancy, France; christo.christov@univ-lorraine.fr
*   Correspondence: marcdiederich@snu.ac.kr; Tel.: +82-2-880-8919
†   These authors equally contributed to this work.

Abstract: Aplysinopsins are a class of marine indole alkaloids that exhibit a wide range of biological activities. Although both the indole and N-benzyl moieties of aplysinopsins are known to possess antiproliferative activity against cancer cells, their mechanism of action remains unclear. Through in vitro and in vivo proliferation and viability screening of newly synthesized aplysinopsin analogs on myelogenous leukemia cell lines and zebrafish toxicity tests, as well as analysis of differential toxicity in noncancerous RPMI 1788 cells and PBMCs, we identified EE-84 as a promising novel drug candidate against chronic myeloid leukemia. This indole derivative demonstrated drug-likeness in agreement with Lipinski's rule of five. Furthermore, EE-84 induced a senescent-like phenotype in K562 cells in line with its cytostatic effect. EE-84-treated K562 cells underwent morphological changes in line with mitochondrial dysfunction concomitant with autophagy and ER stress induction. Finally, we demonstrated the synergistic cytotoxic effect of EE-84 with a BH3 mimetic, the Mcl-1 inhibitor A-1210477, against imatinib-sensitive and resistant K562 cells, highlighting the inhibition of antiapoptotic Bcl-2 proteins as a promising novel senolytic approach against chronic myeloid leukemia.

**Keywords:** aplysinopsin analogs; indole alkaloids; marine source; chronic myeloid leukemia; BH3 mimetics

1. Introduction

Chronic myeloid leukemia (CML) is characterized by the oncogenic *BCR-ABL1* fusion gene expression, which codes for a leukemogenic tyrosine kinase [1]. The first-line therapy for CML is imatinib, a tyrosine kinase inhibitor (TKI) that selectively inhibits the activity of the BCR-ABL fusion protein. Since the discovery of imatinib, the overall survival rate of patients with CML has drastically increased, with patients showing durable responses after imatinib treatment [2]. Leukemia cells, however, develop resistance mechanisms to escape chemotherapy; therefore, despite the high remission rate, a significant number of patients develop resistance or become intolerant to imatinib treatment. Furthermore, 33% of patients who receive imatinib treatment do not achieve a complete cytogenetic response (CCyR) [3]. Thus, alternative strategies for the management of CML are needed to combat chemoresistance, for which compounds of natural origin have shown promise as potential therapeutic agents by their capacity to induce cellular stress mechanisms sensitizing leukemia cells against cytotoxic treatments.

The endoplasmic reticulum (ER) is responsible for protein translocation, proper folding, and protein post-translational modifications [4]. Altered cell metabolism and inflammation may disrupt this balance and result in ER stress that can trigger the unfolded protein response (UPR) [5]. The UPR represents a series of adaptive cellular mechanisms designed to restore protein homeostasis [2], and ER stress activates apoptotic cell death under severe or chronic stress conditions [6]. Autophagy is also a stress-induced cell survival program that involves a catabolic process to degrade large protein aggregates and damaged organelles in autophagosomes [7]. Although autophagy and ER stress function independently, increasing evidence supports that these processes can be coactivated [8].

Aplysinopsin and its derivatives possess rich structural diversity and have been reported to exhibit a wide range of medicinal and biological activities. For example, they act as neuromodulators [9] and possess antineoplastic [9], antiplasmodial [10], and antimicrobial activities [11]. Interestingly, aplysinopsins display cytotoxicity against a range of cancer cell lines [12]. However, their anticancer potential in leukemic cell lines and the corresponding molecular mechanisms remain to be further investigated.

Here we evaluated the anti-leukemic activity of aplysinopsin (EE-115) and analogs EE-31, EE-80, EE-84, and EE-92 (Scheme 1) against chronic myeloid leukemia cell lines. EE-84 exhibited drug-like properties in line with Lipinski's rule of five and showed a stronger cytostatic and cytotoxic effect on leukemia cells than healthy cell models. Furthermore, its safety profile was validated in vivo by using developing zebrafish larvae. Mechanistically, EE-84 induced a senescent-like phenotype in line with its cytostatic activity, triggered autophagy, ER stress, metabolic alterations, and mitochondrial dysfunction. In addition, EE-84 sensitized imatinib-sensitive and -resistant K562 cells against the Mcl-1 inhibitor A-12101477 to induce caspase-dependent apoptosis. Altogether, this study warrants further investigation of the aplysinopsin analog EE-84 as a preclinical drug candidate against chronic myeloid leukemia.
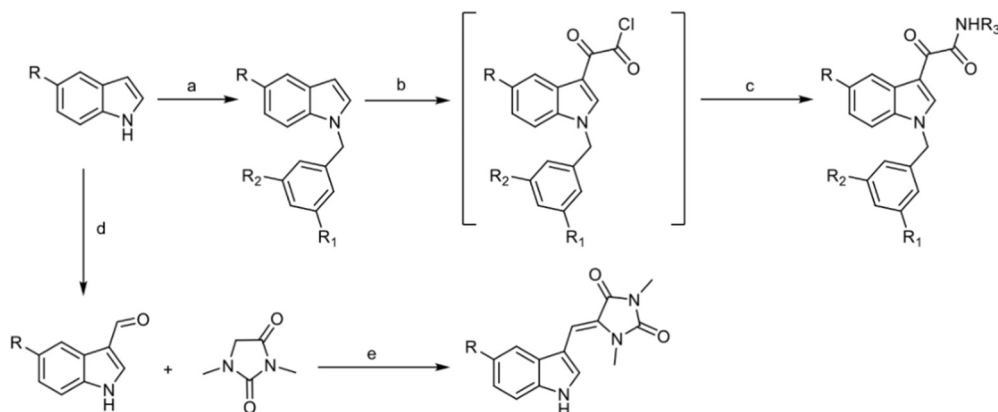

Scheme 1. Synthetic pathway for the preparation of aplysinopsin EE-115 and its analogs EE-31, EE-80, EE-84, and EE-92. Reagents and conditions: (**a**) benzyl chlorides, NaH, DMF; (**b**) oxalyl chloride, dry ethyl ether, heating; (**c**) the reactant amines 2-cyanoacetohydrazide and 1-(2-amino-5-methyl-4,5,6,7-tetrahydrobenzo[b]thiophen-3-yl)ethan-1-one, dry THF, TEA, stirring, 3 h; (**d**) POCl$_3$ DMF, 0 °C, NaOH; (**e**) piperidine, reflux, 4 h.

2. Results

2.1. Aplysinopsin Analogs Display Cytostatic Activities in Myeloid Leukemia Cells

Aplysinopsin (EE-115) and its analogs EE-31, EE-80, EE-84, and EE-92 (Figure 1) were tested for their anti-leukemic effects on the myeloid leukemia cell line K562, using the trypan blue exclusion test (Tables 1 and 2 and Figure S1). NMR spectrum data of ^{1}H of the compounds EE-31, EE-80, EE-84, EE-92, and EE-115 (Figure S2) and ^{13}C NMR spectrum data of the compounds EE-31, EE-80, EE-84, and EE-92 (Figure S3) were provided.
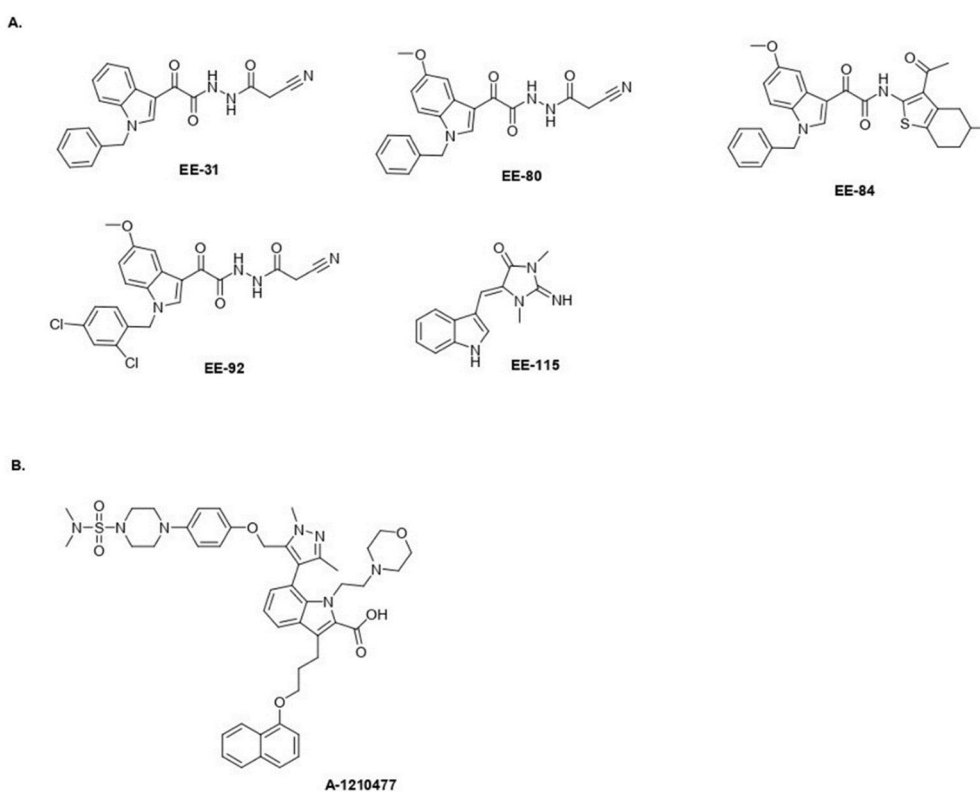
Figure 1. Chemical structures. (**A**) Aplysinopsin (EE-115) and analogs (EE-31, EE-80, EE-84, EE-92). (**B**) A-1210477.

Table 1. GI_{50} of EE-84 in CML cell lines. GI_{50} (μM) values were calculated after indicated times of treatment.

		GI_{50} (μM)		
Compound	**Cell Line**	**24 h**	**48 h**	**72 h**
EE-84	KBM5	>50	33.95 ± 1.89	28.14 ± 1.68
	MEG01	>50	48.40 ± 5.02	28.89 ± 1.52
	K562IR	>100	95.63 ± 16.56	55.09 ± 3.28
	KBM5IR	>100	32.77 ± 2.25	29.15 ± 2.05

GI_{50} values were calculated after trypan blue staining and represent the mean ± S.D. of three independent experiments. GI_{50} indicates the concentration required to cause 50% overall growth inhibition.

Compounds EE-31, EE-80, EE-92, and EE-115 only weakly affected the overall growth (Figure S1A) and viability (Figure S1B) of K562 cells at concentrations up to 50 μM. Interestingly, EE-84 inhibited the growth of K562 with a GI_{50} of 32.22 ± 3.91 μM and 19.07 ± 0.80 μM after 48 and 72 h, respectively (Figure S1A).

Based on the GI_{50} results in the K562 cell line, we selected EE-84 for further investigations compared to EE-115, the parental compound. To generalize the antiproliferative effect of EE-84 in CML, GI_{50} values of EE-84 were calculated on imatinib-sensitive (KBM5, MEG01) and -resistant (IR) (K562IR and KBM5IR) CML cells (Table 1). We next validated the cytostatic profiles of EE-84 by Methocult colony formation assays (CFA) to assess the compounds' effects on the clonogenic potential in a 3D culture environment (Figure 2A–E). EE-84 reduced the total surface area and average size of K562 colonies after a 48-h pretreatment (Figure 2A). Similar results were observed for other CML cell lines (Figure 2A–E).
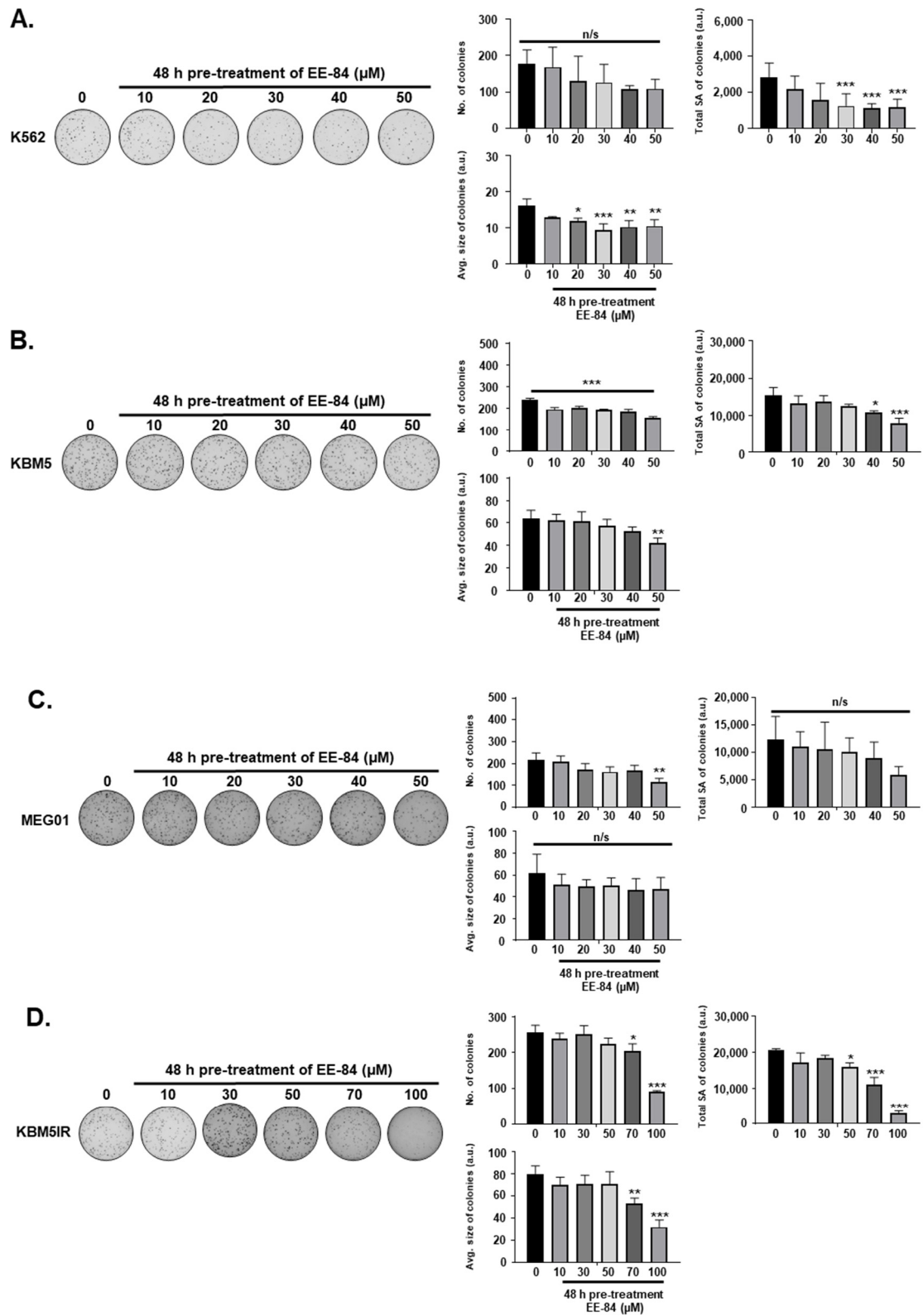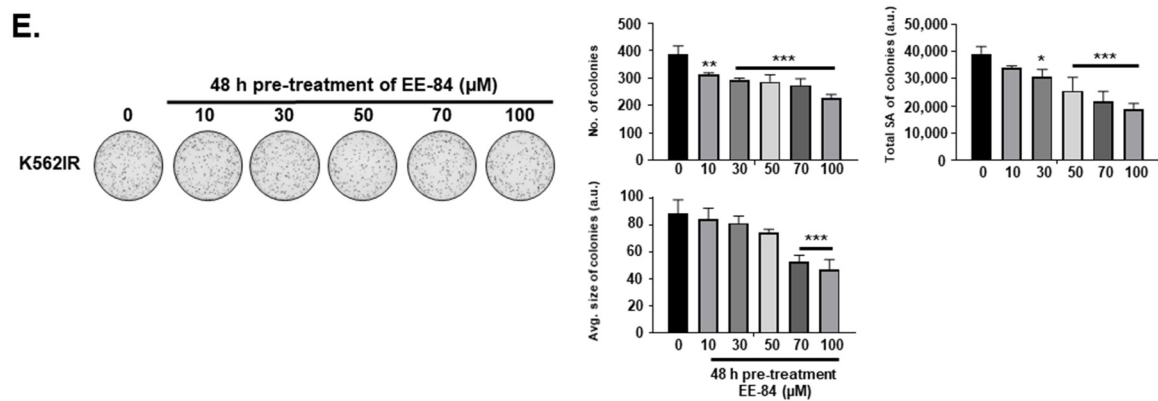
Figure 2. *Cont.*

Figure 2. Differential anti-leukemic effects observed by CFA after aplysinopsin treatments (**A–E**). Representative pictures from three independent experiments of clonogenic assays after 48 h pretreatment of EE-84 (**A**) K562, (**B**) KBM5, (**C**) MEG01, (**D**) KBM5IR, (**E**) K562IR cells are shown on the left. Corresponding quantifications (number of colonies, the total surface area of colonies, and average size of colonies) are indicated on the right. Statistical analysis was performed by one-way ANOVA, followed by Sidak's multiple comparisons test. Differences were considered significant when * $p < 0.05$, ** $p < 0.01$, *** $p < 0.001$ compared to control. n/s: not significant.

Considering the moderate cytotoxic effect of 50 μM EE-84 and EE-115 at 72 h in K562 cells (Figure S1), we quantified cell death induction using Hoechst/PI staining by fluorescent microscopy (Figure 3A). EE-84 reduced K562 cell viability leading to 11.0 ± 4.23% of propidium iodide (PI)-positive cells without nuclear fragmentation. A similar percentage of cell death was shown after quantification of Annexin V APC/PI by FACS (Figure 3B). EE-84 induced approximately 16.5% cell death (Table 2) at the highest concentration of 50 μM. Imatinib (1 μM) was used as a control. Cell cycle analysis showed an accumulation of cells in the sub-G1 phase of 8.34 ± 1.51% after 48 h and 13.03 ± 1.19% after 72 h with EE-84 (50 μM), concomitant with a reduction of the G1 population from 58.40 ± 2.81% at 48 h to 52.03 ± 2.99% at 72 h (Figure 3C and Table 3). Celecoxib (40 μM) was used as a control.

Table 2. Percentage of cell death after treatment of K562 cells with increasing concentrations of EE-84. (Data from Figure 3B).

	EE-84 (μM)						Ima (μM)
	0	**10**	**20**	**30**	**40**	**50**	**1**
AnnV+/PI− (%)	5.12 ± 1.19	7.05 ± 1.46	5.60 ± 1.98	6.65 ± 2.29	7.71 ± 2.10	8.22 ± 3.12	51.77 ± 2.29
AnnV+/PI+ (%)	2.68 ± 0.77	2.50 ± 0.62	4.40 ± 0.94	7.51 ± 2.70	8.97 ± 1.03	8.25 ± 1.95	31.27 ± 5.24
Combined cell death (%)	7.80 ± 1.73	9.55 ± 3.22	10.00 ± 0.85	14.16 ± 0.61	16.68 ± 0.89	16.46 ± 0.02	83.03 ± 14.50

Results are the mean ± S.D. of three independent experiments.
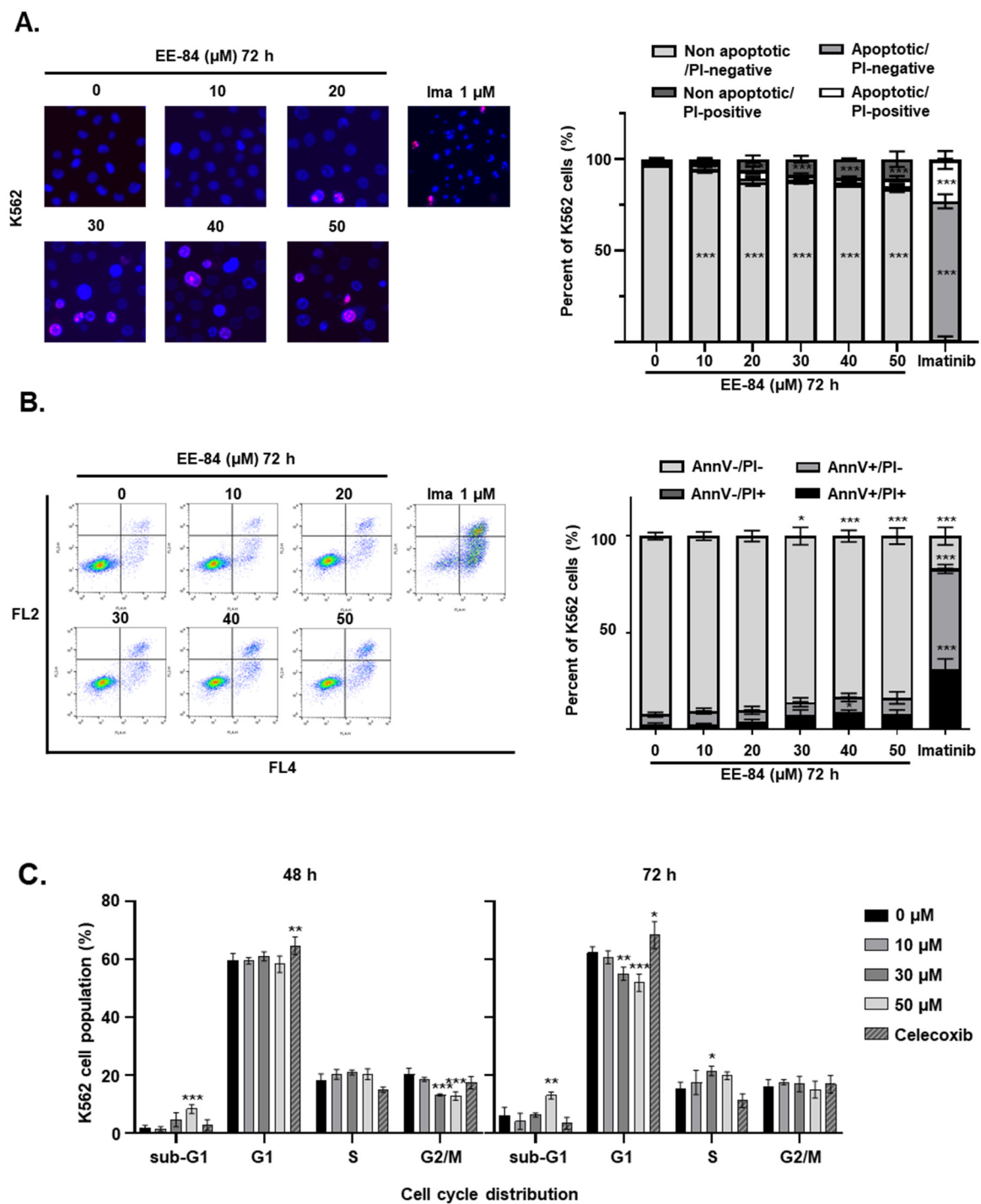
Figure 3. Percentage of cell death after increasing concentrations of EE-84 treatment in K562 cells. (**A**) Representative microscopy images of Hoechst 33342/PI double-stained nuclei of K562 cells exposed to different concentrations of aplysinopsin derivatives at indicated times are shown. The percentage of apoptotic cells was calculated from three independent experiments. (**B**) Results obtained after Annexin V APC/PI staining and quantification by FACS. Ima: imatinib (1 μM). (**C**) For cell cycle analysis, K562 cells were treated with 10, 30, and 50 μM EE-84 for 48 and 72 h. Cell cycle phase distribution was determined by FACS. All data were expressed as mean ± SD of three independent experiments. Statistical analysis was performed by two-way ANOVA, followed by Dunnett's multiple comparisons test (Microscopy, Cell cycle); by Sidak's multiple comparisons test (Annexin V/PI); * $p < 0.05$, ** $p < 0.01$, *** $p < 0.001$ compared to controls.

Table 3. Cell cycle phase distribution after treatment of K562 cells with increasing concentrations of EE-84. (Data from Figure 3C).

48 h Treatment	EE-84 (μM)				Celecoxib (μM)
%	0	10	30	50	40
Sub-G1	1.78 ± 0.91	1.48 ± 0.81	4.65 ± 2.42	8.34 ± 1.51	2.79 ± 1.90
G1	59.81 ± 2.29	59.59 ± 1.12	61.11 ± 1.58	58.40 ± 2.81	64.77 ± 3.09
S	18.02 ± 2.49	20.30 ± 1.68	20.99 ± 0.83	20.41 ± 1.84	15.00 ± 0.93
G2/M	20.39 ± 2.12	18.64 ± 0.75	13.25 ± 0.32	12.86 ± 1.46	17.44 ± 2.13
72 h Treatment	EE-84 (μM)				Celecoxib (μM)
%	0	10	30	50	40
Sub-G1	6.07 ± 2.88	4.08 ± 2.80	6.33 ± 0.74	13.03 ± 1.19	3.41 ± 2.04
G1	62.33 ± 2.13	60.83 ± 2.33	55.09 ± 2.26	52.03 ± 2.99	68.43 ± 4.67
S	15.50 ± 2.14	17.52 ± 4.24	21.55 ± 1.64	19.85 ± 1.33	11.20 ± 2.37
G2/M	16.10 ± 2.50	17.57 ± 0.90	17.03 ± 2.69	15.08 ± 2.89	16.96 ± 3.04

Results are the mean $\pm$ S.D. of three independent experiments.

### 2.2. Drug-Likeness of Compounds EE-84 and EE-115

Next, we examined the drug-likeness of the two compounds according to Lipinski's rule of five (Table 4) [13]. A molecule is orally active when there are no more than 5 H bond donors and no more than 10 H bond acceptors, when the molecular mass is less than 500 Daltons, and when the octanol–water partition coefficient LogP is not greater than 5. EE-115 did not violate any of the conditions mentioned above. For EE-84, The LogP corresponds to 5.91; however, this aplysinopsin derivative can still be considered a drug-like candidate since one exception is acceptable.

Table 4. In silico prediction for the drug-likeness of EE-84 and EE-115. Drug-likeness of the aplysinopsin derivatives were calculated and interpreted based on Lipinski's rule of five.

	EE-84	EE-115
Mass	500.00	254.00
Hydrogen bond donor	1	2
Hydrogen bond acceptor	5	4
LogP	5.91	1.85
Molar reactivity	142.51	74.54

2.3. Effect of EE-84 and EE-115 on Healthy Cells and Zebrafish Embryos

We then assessed the effect of EE-84 and EE-115 on healthy models. Even though EE-84 affected the proliferation of RPMI 1788 cells dose-dependently (Figure S4A), this modulation was evident at later times (as early as 72 h vs. 48 h in cancer cells), with a higher GI_{50} (40.10 ± 3.79 in RPMI 1788 vs. 19.07 ± 0.80 μM after 72 h in K562 cells; Tables 1 and 5). Altogether, EE-84 generated significant differential toxicity of RPMI-1788/K562 cells at 40 and 50 μM (Figure 4A). On the other hand, EE-115 inhibited the growth of normal RPMI 1788 cells (Table 5) more than K562 cells (Figure S4A). Moreover, EE-84 did not significantly affect the viability of RPMI 1788 cells, whereas EE-115 reduced the viability of RPMI 1788 cells at the highest concentrations (Table S1 and Figure S4B). Altogether EE-84 appeared to have a more advantageous safety profile.
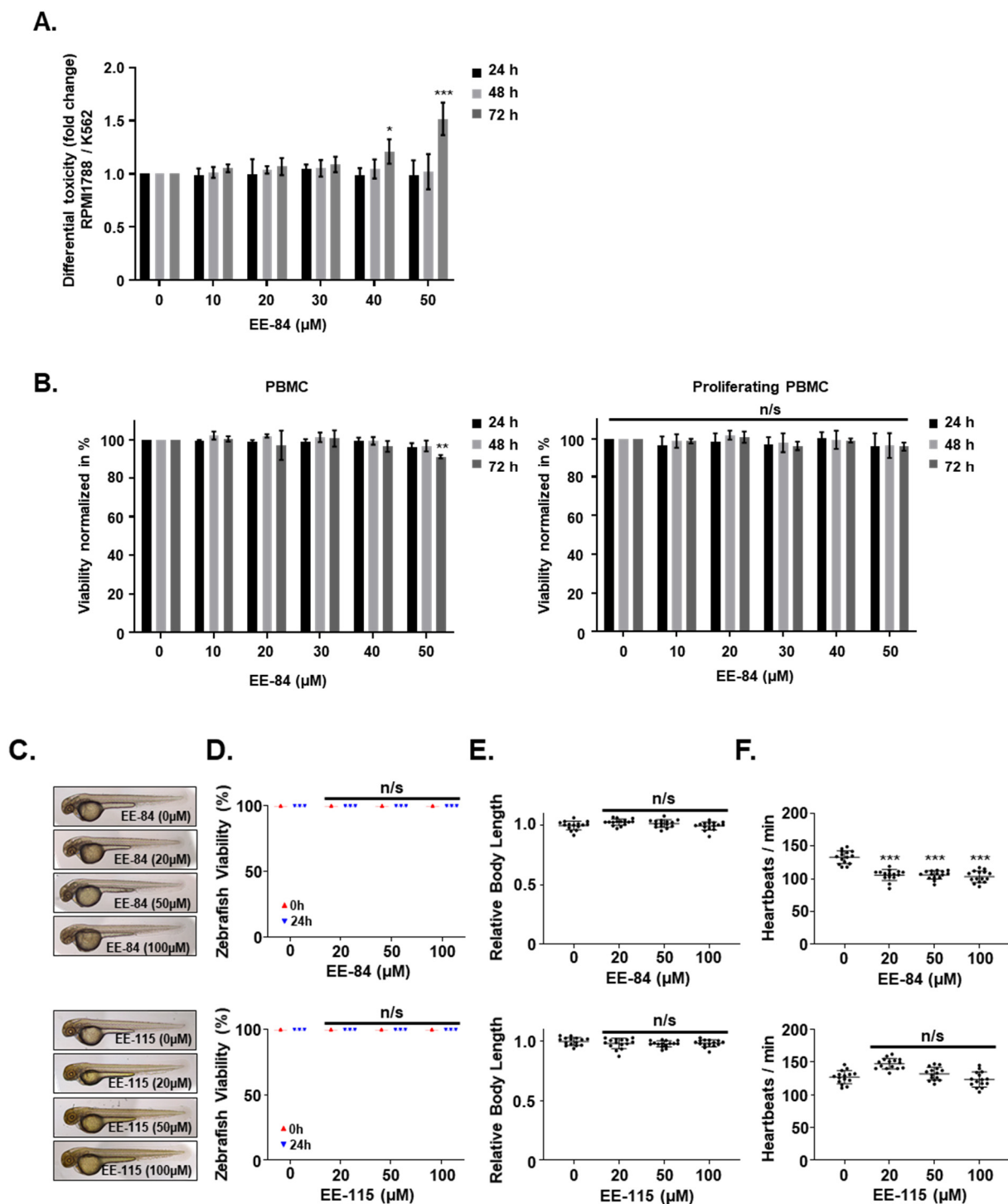
Figure 4. Effect of aplysinopsin derivatives on healthy cell models. (**A**) Differential toxicity (RPMI 788/K562) of EE-84 was determined by the trypan blue exclusion test. (**B**) Toxicity test of EE-84 in nonproliferating and proliferating PBMCs. After 24, 48, and 72 h of EE-84 treatment, viability was determined by the trypan blue exclusion test. Zebrafish toxicity assays were performed by treatment with aplysinopsins at indicated concentrations. (**C**) Representative pictures of zebrafish are shown. Zebrafish viability (**D**), relative body length (**E**), and heartbeats/min (**F**) were measured. Data represents a total of 15 fish per group. Trypan blue exclusion test data represents the mean ± SD of three independent experiments. Statistical analysis: two-way ANOVA with Dunnett's multiple comparison test (trypan blue exclusion test); * $p < 0.05$, ** $p < 0.01$, *** $p < 0.001$ compared to controls. Ordinary one-way ANOVA followed by Dunnett's post hoc test (Zebrafish assay) revealed significant differences indicated by *** $p < 0.001$ compared to control. n/s: not significant.

Table 5. GI_{50} of aplysinopsins on RPMI 1788. GI_{50} (μM) values were evaluated after indicated times of compound treatment.

	GI_{50} (μM)		
Compound	24 h	48 h	72 h
EE-84	>50	>50	40.10 $\pm$ 3.79
EE-115	>50	30.36 $\pm$ 1.95	27.72 $\pm$ 2.30

GI_{50} values were calculated after trypan blue staining and represent the mean $\pm$ S.D. of three independent experiments. GI_{50} indicates the concentration required to cause 50% overall growth inhibition.

We generalized our findings and validated the absence of cytotoxic/cytostatic effects of EE-84 on nonproliferating and proliferating peripheral blood mononuclear cells (PBMCs) from healthy donors. In addition, EE-84 did not induce toxic effects in any of the two cell models (Figure 4B).

We then treated zebrafish embryos 24 h post-fertilization (hpf) to validate the in vivo safety profiles of the aplysinopsin compounds EE-84 and EE-115. The zebrafish were observed after 24 h of exposure to different concentrations of aplysinopsins. No significant morphological changes were notable at the different concentrations of the compounds used (Figure 4C). Concentrations up to 100 μM of EE-84 and EE-115 did not affect the survival rate (Figure 4D) or growth (Figure 4E) of the treated zebrafish. A moderate decrease in the heart rate (Figure 4F) was noted for EE-84.

Altogether, based on these results, we further investigated the molecular and cellular effects of EE-84, considering the observed differential toxicity.

2.4. EE-84 Induced Morphological Changes and Cell Stress Responses in CML Cells

EE-84 (50 μM) increased the cell size (Figure 5A) and the number of intracellular vacuoles up to 96 h. These morphological changes were quantified by flow cytometry (Figure 5B). Compared to DMSO-treated controls, EE-84-treated K562 cells showed a progressive increase in forward scatter values (FSC-H; a.u.) and side scatter (SSC-H; a.u.) as measurements of cell size and granularity, respectively. The increase in cell size and granularity and the cytostatic effects were considered part of a cellular stress response driving cells into senescence. We then examined the senescent-like phenotype using stress-associated (SA)-β-galactosidase staining. We measured increased cell size and SA-β-gal positive cells after treatment with EE-84 at 50 μM for 72 h. Doxorubicin (80 nM), known to induce senescence, was used as a bona fide control (Figure 5C).

In addition, morphological changes were examined by transmission electron microscopy (TEM). K562 cells treated with EE-84 underwent mitochondrial damage after 24, 48, and 72 h of compound exposure as well as mitophagy (Figure 5D). In addition, we assessed the mitochondrial metabolism in K562 after treatment with EE-84 at 30 μM for 72 h by using the Agilent Seahorse XFp Cell Mito Stress test. The oxygen consumption rate (OCR) significantly decreased after treatment with EE-84 compared to control (Figure 5E). Thus, our results confirmed that EE-84 induced cell stress and reduced mitochondrial activity in agreement with morphological alterations of the mitochondria observed by TEM.
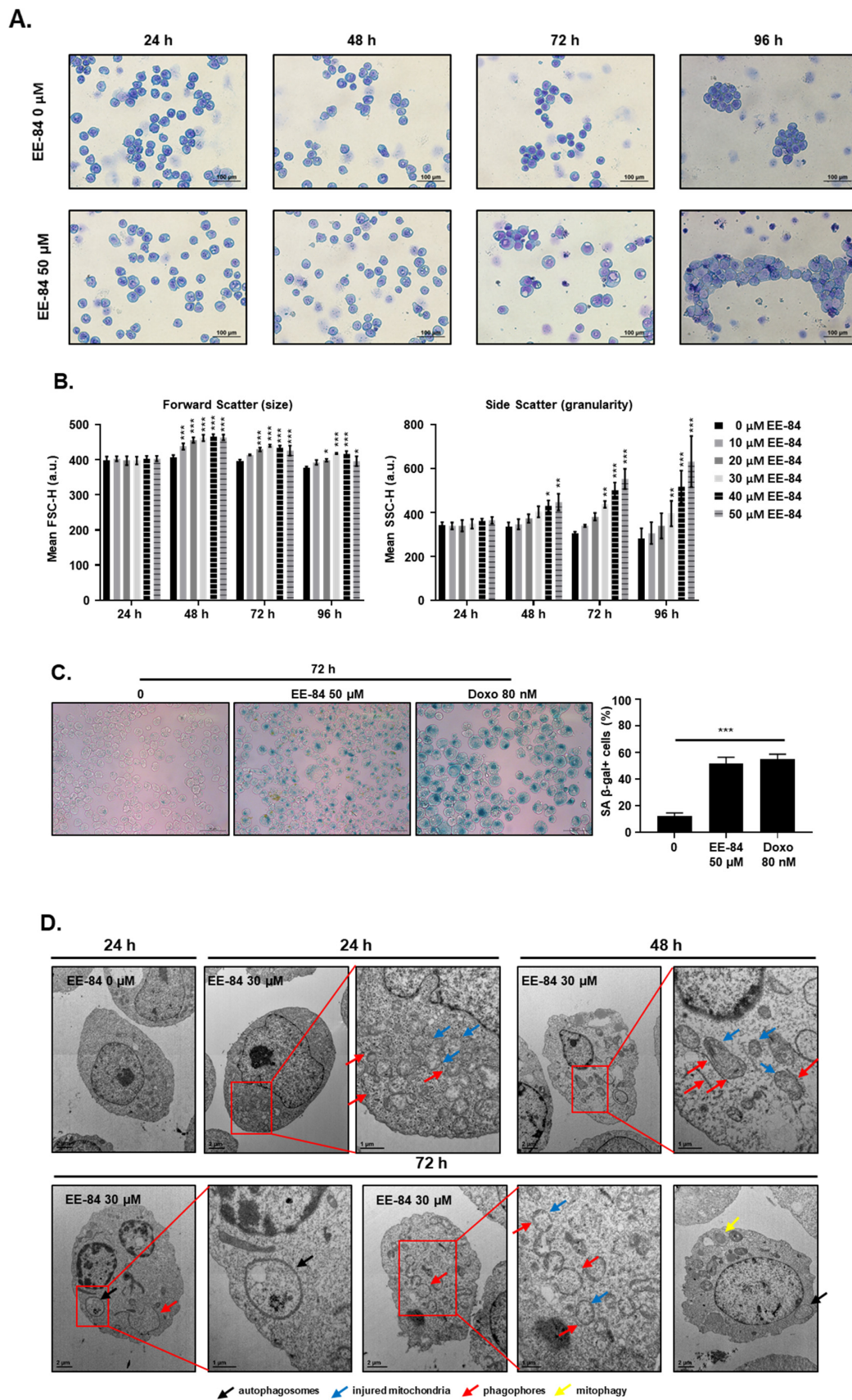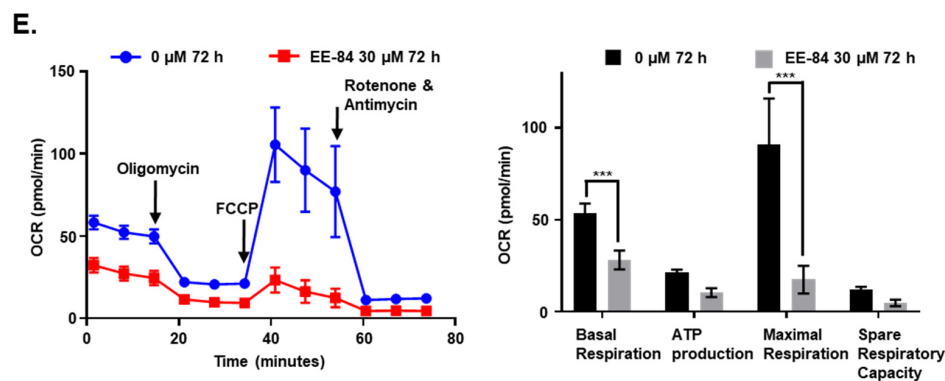
Figure 5. *Cont.*

Figure 5. Morphological changes of K562 cells treated with EE-84. (**A**) K562 cells were treated with 50 μM EE-84 for 24, 48, 72, and 96 h. Light microscopy at magnification 200× was used for morphological observation. (**B**) K562 cells were treated with indicated concentrations of EE-84 for up to 96 h. At the indicated time points, cells were harvested and analyzed by flow cytometry using forward (relative cell sizes; FSC-H) and side scatter (granularity; SSC-H) measurements. For morphological analysis of EE-84, exposed K562 cell debris were excluded. (**C**) SA-β-gal staining of the K562 cells treated with 50 μM of EE-84 for 72 h. The quantitative analysis of the incidence of the cells with positive β-gal staining. Doxo: doxorubicin (80 nM). (**D**) Transmission electron microscopy at magnifications of 8000× or 10,000× (whole cells) and 20,000× or 25,000× (cell details). Cells were treated with 30 μM EE-84 and were exposed for up to 72 h. Phagophores, autophagosomes, injured mitochondria, and incidence of mitophagy were highlighted using red, black, blue, and yellow arrows, respectively. DMSO-treated K562 cells at 24 h were used as control. (**E**) Measurement of mitochondrial function in K562 cells. The experiments were conducted using the Seahorse XFp Cell Mito Stress test, and the OCR measurement is visualized. Results are the mean ± SD of three independent experiments. Statistical analysis was performed by two-way ANOVA, followed by Dunnett's multiple comparisons test (Cell size by FACS); by Tukey's multiple comparisons test (Senescence); by Sidak's multiple comparisons test (Seahorse XFp Cell Mito Stress test); * $p < 0.05$, ** $p < 0.01$, *** $p < 0.001$ compared to controls.

2.5. Autophagy and Endoplasmic Reticulum (ER) Stress Were Triggered by EE-84 as Cellular Stress Responses in K562 Cells

Autophagy is a catabolic pathway activated in response to different cellular stressors, such as damaged organelles, accumulation of misfolded or unfolded proteins, ER stress, and DNA damage [14]. Based on the TEM results, we then investigated the expression levels of the microtubule-associated protein-1 light chain 3 (LC3I) conversion to the phosphatidylethanolamine-conjugated form of LC3I (LC3II) by Western blot. Results showed that levels of LC3 II gradually increased over time after treatment with EE-84 at 30 μM in K562 at 24, 48, and 72 h, respectively (Figure 6A). In addition, we observed the formation of cytoplasmic vacuoles in EE-84 treated K562 cells after 48 h at 30 μM by Diff-Quik staining, suggestive of autophagy induction. To validate the involvement of EE-84 in autophagy induction, we post-treated bafilomycin A1 (Baf-A1), an inhibitor of the vacuolar-type H⁺-ATPase which blocks the late phase of autophagy by preventing lysosomal acidification, at 40 nM for 8 h (cells were treated or not with EE-84 for 40 h before addition of Baf-A1 for 8 h), resulting in significant inhibition of vacuole formation after 48 h at 30 μM EE-84 (Figure 6B). To see the effect of autophagy inhibition on cell viability, we conducted a trypan blue assay test of EE-84 treated K562 cells with or without Baf-A1 post-treatment. 89.0% of cell viability was observed in EE-84 treated K562 cells with Baf-A1 post-treatment compared to 98.7% of cell viability in EE-84 treated K562 cells alone (Figure 6B).

In addition, studies have shown that autophagy and endoplasmic reticulum (ER) stress are closely related [8]. ER stress is considered a protective stress response in eukaryotic cells [15]. We then assessed whether EE-84 induces ER stress and subsequently regulates autophagy. We measured sensor proteins such as PERK, ATF6, and GRP78 that play a role in activating the unfolded protein response (UPR) in response to ER stress. PERK and phosphorylated eIF2α were significantly increased after treatment with EE-84 at 30 and 50 μM in K562 cells after 72 h. The abundance of ATF4, an effector of PERK and eIF2α,

also increased, which indicated that the PERK-eIF2α-ATF4-CHOP pathway was activated under EE-84-induced ER stress (Figure 6C). Since GRP78 is involved in glycolysis [16], we then assessed the glycolytic flux levels in K562 after treatment with EE-84 at 50 μM for 72 h by using the Agilent seahorse XFp Glycolysis Stress test. The glycolysis and glycolytic capacity measured by the extracellular acidification rate (ECAR) significantly decreased after treatment with EE-84 compared to control (Figure 6D). We also confirmed the glycolytic flux levels in K562IR cells after treatment with EE-84 at 100 μM for 72 h. The results showed that the glycolytic capacity of ECAR also significantly decreased after treatment with EE-84 (Figure S5). Altogether, these data demonstrated that the prolonged treatment with EE-84 induced the PERK-eIF2α-ATF4-CHOP UPR pathway involved in EE-84-induced autophagy.
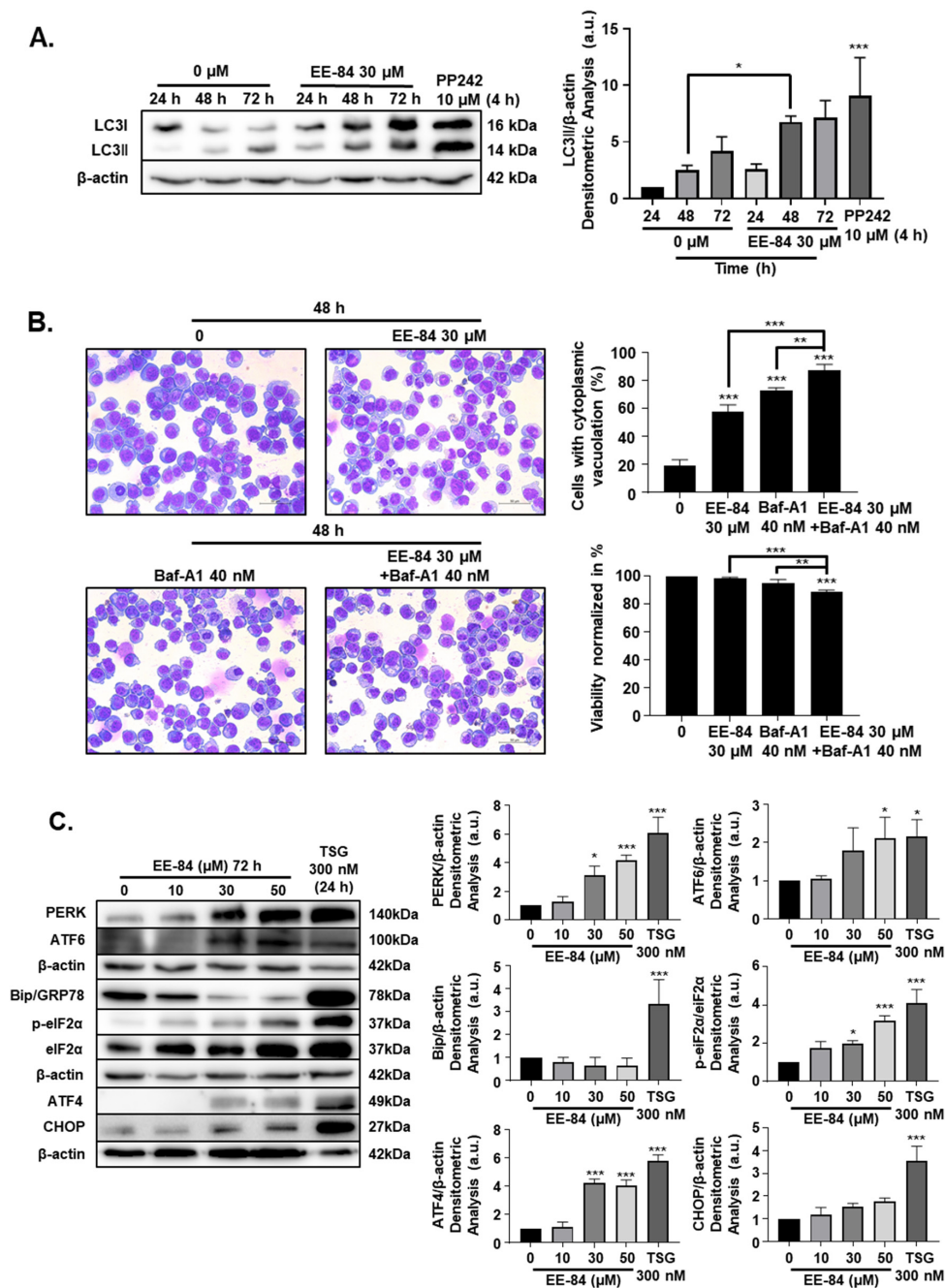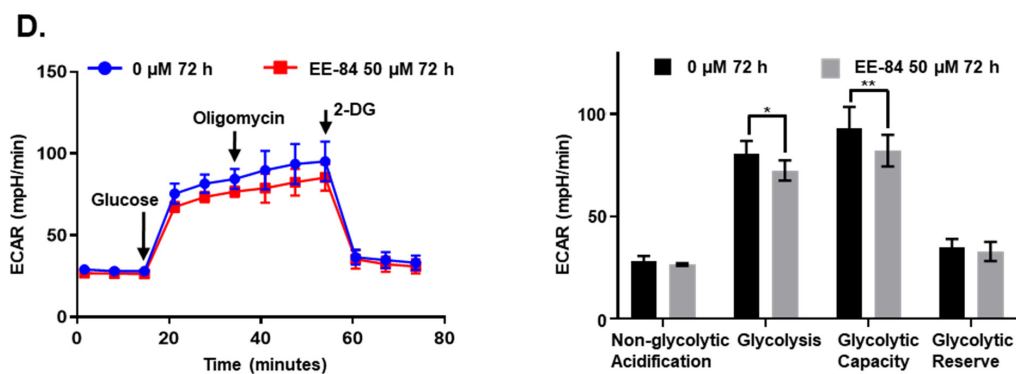

Figure 6. *Cont.*

Figure 6. EE-84 induced autophagy and ER stress. (**A**) K562 cells were treated with 30 μM EE-84 for 24, 48, and 72 h. Western blot analysis of the LC3B protein. B-actin was used as a loading control. Quantification of LC3B protein bands through normalization by β-actin protein bands. (**B**) Diff-Quik staining of K562 cells after 48 h of EE-84 treatment (30 μM) with or without Baf-A1 post-treatment. Baf-A1: bafilomycin A1 (40 nM). (**C**) ER stress-related proteins were detected by Western blot analysis. B-actin was used as a loading control. After quantifying the bands, p-eiF2α levels were normalized to total eIF2α, and all other proteins were normalized to β-actin. TSG: thapsigargin (300 nM). (**D**) Measurement of glycolytic capacity in K562 cells. 2-DG: 2-deoxy-D-glucose. The experiments were conducted using the Seahorse XFp Glycolysis Stress test, and the flow chart and bar graph show the measurement of ECAR. Results are the mean ± SD of three independent experiments. Statistical analysis was performed by two-way ANOVA, followed by Tukey's multiple comparisons test (autophagy Western blot, Diff-Quik staining); by Dunnett's multiple comparisons test (ER stress Western blot); by Sidak's multiple comparisons test (Seahorse XFp Glycolysis Stress test); * $p < 0.05$, ** $p < 0.01$, *** $p < 0.001$ compared to controls.

2.6. EE-84 Sensitized K562 Cells against Mcl-1 Inhibitor A-1210477 and Showed Synergistic Cytotoxicity in K562 and K562IR Cells

Conditions of ER stress may promote Mcl-1 protein stabilization via mechanisms involving UPR and ATF4 upregulation [17,18]. Considering the cytostatic potential but limited cytotoxicity of EE-84 along with the induction of ER stress, we then investigated the expression levels of the antiapoptotic protein, Mcl-1, which may be responsible for the apoptotic blockage. Based on the increase of antiapoptotic Mcl-1 expression in EE-84-treated K562 cells after 24 h compared to control (Figure 7A), we speculated that the combined treatment of the specific Mcl-1 inhibitor A-1210477 with EE-84 might sensitize K562 cells to apoptotic cell death. Using subtoxic concentrations of EE-84 (20 and 30 μM) and A-1210477 (10 μM), we first assessed the combinatory effects of these compounds using Hoechst/PI staining after 24 h (Figure 7B). We observed 46.89 ± 21.84% and 56.00 ± 25.46% induction of apoptotic cell death in combinatory treatments. The combination index (CI) of each compound-pair was calculated, and the combinatory treatment showed a synergistic effect (Figure 7C and Table 6). We also compared viability between EE-84 alone and in combination with A-1210477 after 24 h (Table 7). Our results showed that the Mcl-1-specific inhibitor A-1210477 sensitized EE-84-treated K562 and K562IR cells. Next, we confirmed the apoptotic cell death mechanism triggered by the combination treatment. As shown in Figure 7D, about 14.5% of apoptotic cell death was induced by A-1210477 alone, whereas over 40% of apoptosis was observed by a combination of EE-84 and A-1210477 after 24 h. z-VAD pretreatment completely prevented apoptosis induction in K562 cells in single and combined treatments (Figure 7D). The caspase-dependent nature of cell death modality was also confirmed by Annexin V APC/PI staining after 24 h in K562 cells (Figure 7E). Results showed that EE-84 (30 μM) in combination with A-1210477 (10 μM) induced 23.03 ± 4.08% early apoptosis (AnnV+/PI−) and 23.07 ± 5.32% late apoptosis (AnnV+/PI+) in K562 cells after 24 h of treatment (Table 8). Again, zVAD completely protected against cell death in all instances. Imatinib (1 μM) was used as a control. In addition, the cytotoxic effect of subtoxic concentrations of EE-84 (30 and 50 μM) in combination with A-1210477 (20 μM) was also tested on K562IR cells after 24 h of treatment, using the trypan blue exclusion test (Figure 7F). Results showed that viability was reduced by 25.4% when cells were

cotreated with 20 µM A-1210477 and 30 µM of EE-84. A co-treatment with 50 µM EE-84 and 20 µM A-1210477 induced 40% of cell death. We further confirmed the combinatory effects of these compounds using Annexin V APC/PI staining after 24 h in K562IR cells (Figure 7G). Altogether, our results indicated that the specific Mcl-1 inhibitor A-1210477 sensitized K562 and K562IR cells to EE-84, significantly increasing cell death induction. Since mitochondrial dysfunction can trigger apoptosis, we measured the percentage of mitochondrial membrane potential (MMP) loss due to the combined effects of EE-84 with A-1210477 in K562 after 24 h. Results showed that the percentage of MMP loss significantly increased in K562 after cotreatment with EE-84 and A-1210477 (Figure 7H). In addition, we confirmed the combination effects of EE-84 with A-1210477 in K562 by colony formation assays (CFA); EE-84 combined with A-1210477 reduced the number of colonies, the total surface area, and the average size of colonies in K562 (Figure 7I). The obtained values for the two compound combinations denoted synergism, and 30 µM of EE-84 with 10 µM of A-1201477 were selected for further investigations.

Table 6. Combination indexes obtained by Compusyn software after treatment of K562 with EE-84 and A-1201477.

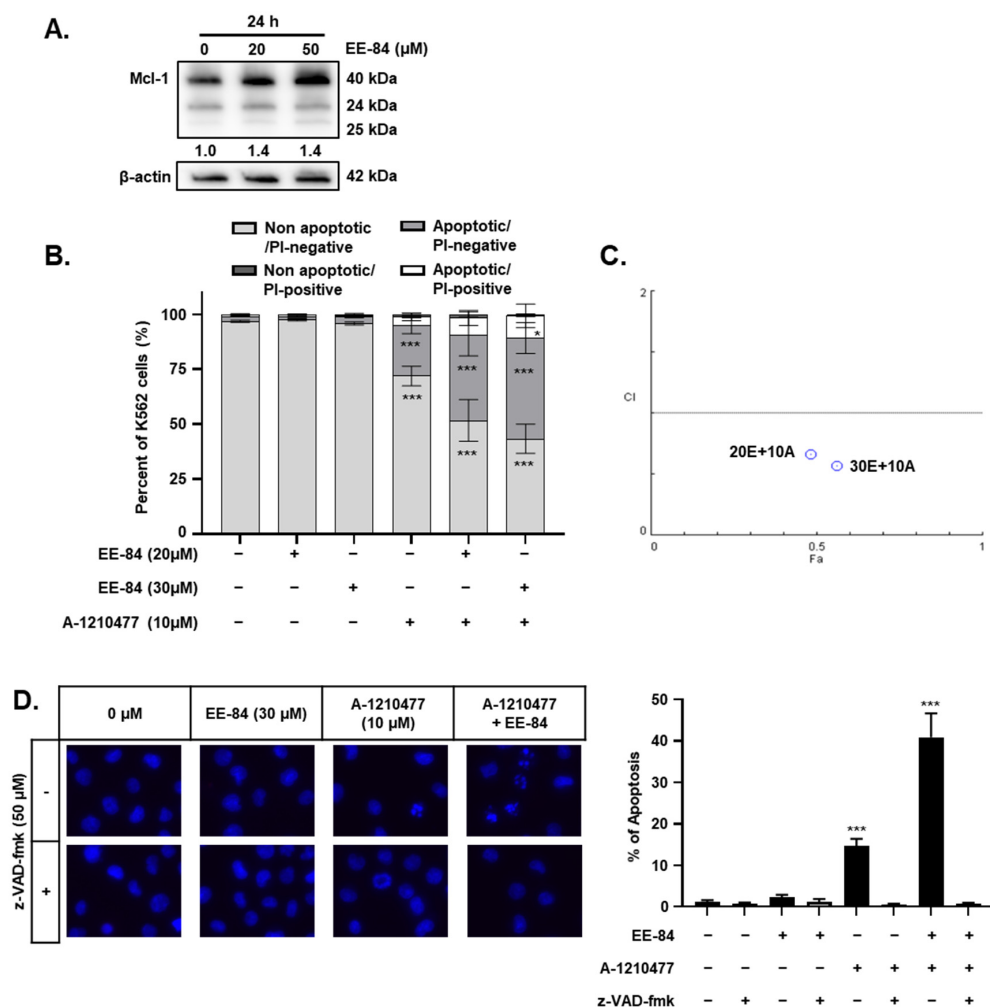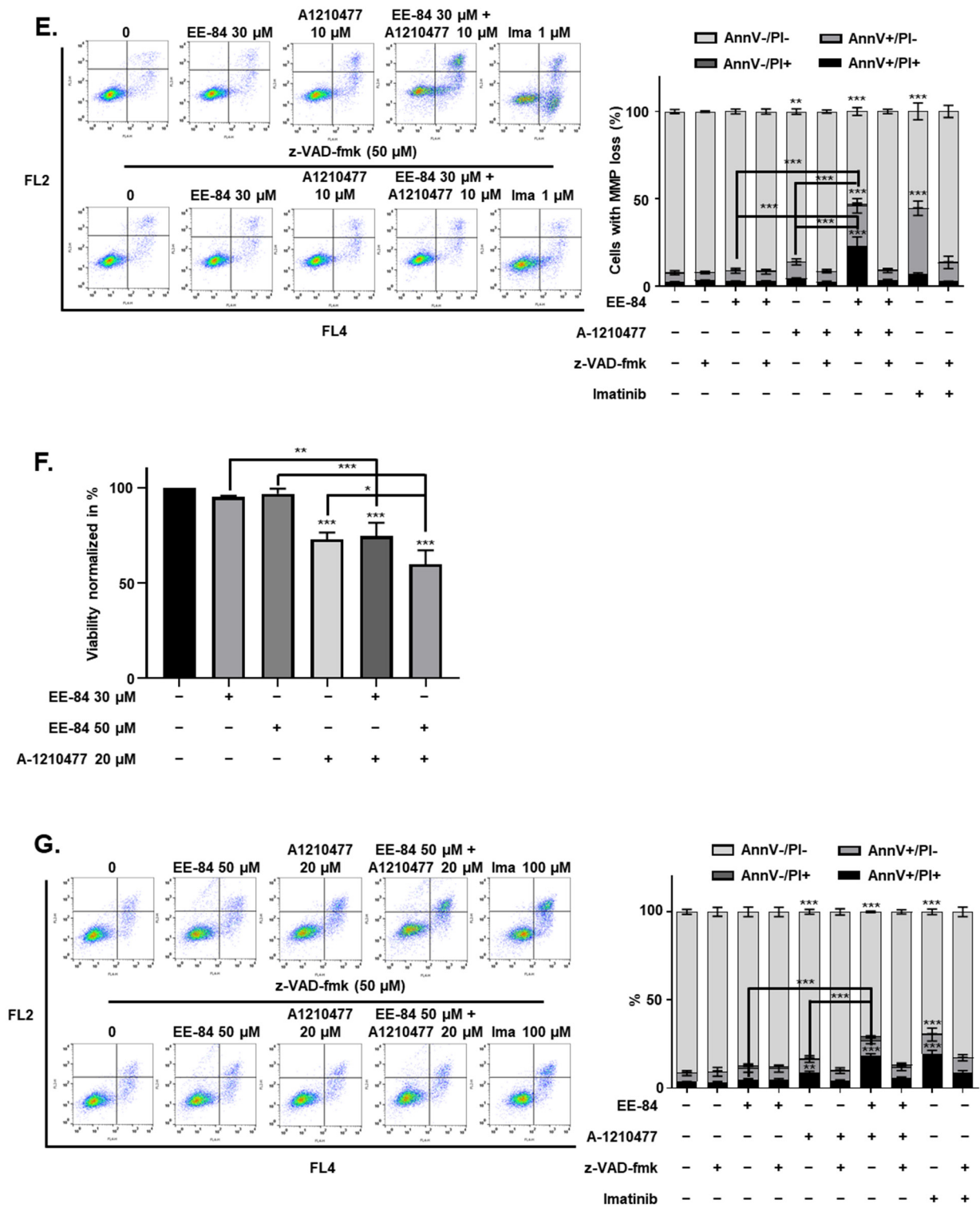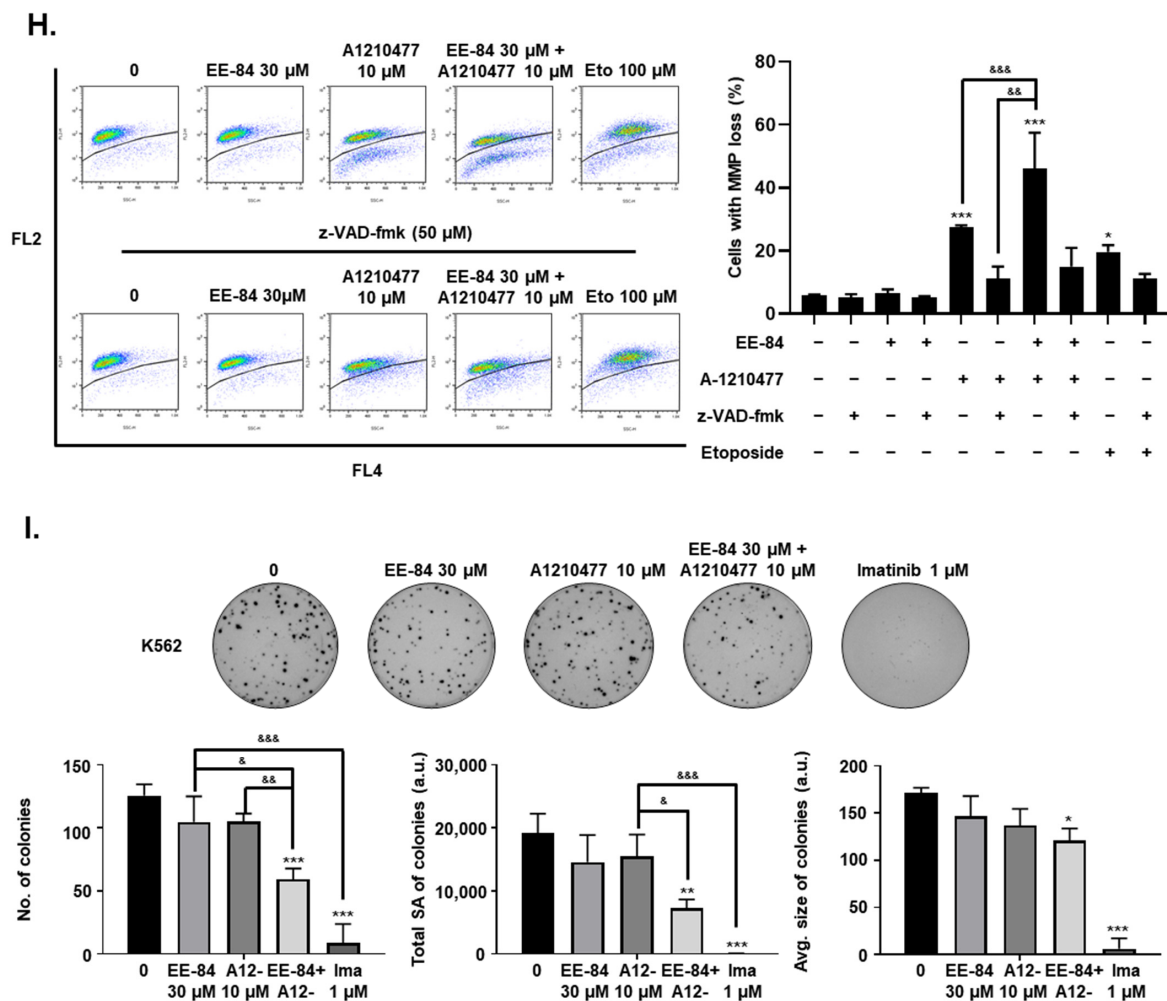| EE-84 (µM)	A-1210477 (µM)	Fa	CI
20	10	0.483	0.66
30	10	0.563	0.57

Figure 7. *Cont.*

Figure 7. *Cont.*

Figure 7. EE-84 sensitized CML cells to BH3 mimetics. (**A**) EE-84 increased expression levels of antiapoptotic protein Mcl-1 compared to DMSO-treated control. K562 cells were treated with varying concentrations of EE-84 for 24 h. The effects on Mcl-1 and β-actin were determined by Western blot analysis. Western blot data interpreted in terms of fold changes in protein expression compared to control at the corresponding time point. The values represented the average of three independent experiments. (**B**) Cotreatment analysis of 20 and 30 μM EE-84 with 10 μM A-1210477 using Hoechst 33258/PI staining showed an increase in apoptotic cell death compared to single treatments of compounds after 24 h in K562 cells. (**C**) The plot representing the fraction affected-combination index (Fa-CI) of the treatment of K562 cells with EE-84 and A-1210477 after 24 h was obtained with Compusyn software. (**D**) The optimal compound combination of 30 μM EE-84 and 10 μM A-1210477 was analyzed by Hoechst/PI staining. z-VAD-fmk was used as a pan-caspase inhibitor. (**E**) The compound combination of 30 μM EE-84 and 10 μM A-1210477 treated K562 cells after 24 h. After 24 h of treatment, the type of cell death triggered by EE-84 with or without A-1210477 was characterized by FACS after Annexin V APC/propidium iodide (PI) staining. Pictures are representative of three independent experiments (**left panel**), and the corresponding quantification (**right panel**) is shown. Ima: imatinib (1 μM). (**F**) K562IR cell viability by trypan blue exclusion assay. (**G**) Annexin V APC/PI staining of K562IR analyzed by FACS. Results are the mean ± SD of three independent experiments. (**H**) Mitochondrial membrane potential (MMP) of the combination of 30 μM EE-84 and 10 μM A-1210477 was analyzed by FACS, and the percentage of cells exhibiting MMP loss was calculated (**right panel**). z-VAD-fmk was used as a pan-caspase inhibitor. Eto: etoposide (100 μM). (**I**) Differential anti-leukemic effects observed by CFA after EE-84 treatments with A-1210477 on K562. Corresponding quantifications (the number of colonies, the total surface area of colonies, and the average size of colonies) are indicated on the right. Results are the mean ± SD of three independent experiments. Statistical analysis was performed by one-way or two-way ANOVA, followed by Dunnett's multiple comparisons test (Microscopy), by Tukey's multiple comparisons test (colony formation assay, MMP, Annexin V/PI); * $p < 0.05$, ** $p < 0.01$, *** $p < 0.001$ compared to controls, & $p < 0.05$, && $p < 0.01$, &&& $p < 0.001$ between indicated conditions.

Table 7. Viability of K562 and K562IR cells (%) after treatment with EE-84 alone or in combination with A-1210477. Viability (%) was calculated after indicated times of compound treatment.

		Viability (24 h)	
Treatment	**Cell Line**		**%**
EE-84 (30 μM)	K562		98.0 ± 1.0
	K562IR		95.3 ± 0.6
EE-84 (50 μM)	K562		96.0 ± 0.7
	K562IR		97.0 ± 2.7
A-1210477 (10 μM)	K562		79.3 ± 1.5
A-1210477 (20 μM)	K562IR		73.0 ± 3.6
EE-84 (30 μM) + A-1210477 (10 μM)	K562		69.0 ± 3.0
EE-84 (30 μM) + A-1210477 (20 μM)	K562IR		74.7 ± 7.1
EE-84 (50 μM) + A-1210477 (20 μM)	K562IR		60.0 ± 7.2

Results are the mean ± S.D. of three independent experiments.

Table 8. Cell death induction (%) after treatment with EE-84 alone or in combination with A-1210477. (Data represent Figure 7E).

	0	EE-84 30 μM	A-121047710 μM	EE-84 30 μM +A-121047710 μM	Ima 1 μM
AnnV+/PI− (%)	5.36 ± 1.14	6.00 ± 1.43	9.31 ± 1.78	23.03 ± 4.08	37.77 ± 4.07
AnnV+/PI+ (%)	2.53 ± 0.28	2.98 ± 0.23	4.73 ± 0.17	23.07 ± 5.32	6.97 ± 0.88
Combined cell death (%)	7.90 ± 2.00	8.98 ± 2.14	14.04 ± 3.24	46.10 ± 0.02	44.74 ± 21.78
z-VAD-fmk (50 μM)					
	0	EE-84 30 μM	A-121047710 μM	EE-84 30 μM +A-121047710 μM	Ima 1 μM
AnnV+/PI− (%)	4.46 ± 0.68	5.33 ± 1.35	6.04 ± 0.99	5.24 ± 1.15	10.86 ± 3.57
AnnV+/PI+ (%)	3.61 ± 0.13	3.13 ± 0.21	2.81 ± 0.21	3.84 ± 0.28	2.93 ± 0.15
Combined cell death (%)	8.07 ± 0.60	8.46 ± 1.55	8.85 ± 2.28	9.08 ± 0.99	13.79 ± 5.60

Results are the mean ± S.D. of three independent experiments.

2.7. Synergistic Induction of Caspase-Dependent Apoptosis by Combination Treatment of EE-84 and A-1210477 in K562 Cells

The cytotoxic effect and caspase-dependent apoptotic activity of the combination treatment were also validated by quantification of intracellular ATP levels. ATP levels decreased significantly after combination treatments compared to the compounds alone (Figure 8A). The 1 h pretreatment of z-VAD-fmk showed an increase in cell viability with the single treatment of 10 μM A-1210477 and the combined treatment. The addition of the caspase inhibitor showed no significant difference in the ATP levels for the single treatment of 30 μM EE-84. To further validate our data, the activity of caspase-3/7 was measured. There was a significant increase in the caspase-3/7 activity by 5.52-fold after the combined treatment of EE-84 and the Mcl-1 inhibitor compared to the untreated control (Figure 8B). To examine the detailed mechanism by which the combined treatment acts, we studied the intrinsic and extrinsic apoptotic pathways in K562 cells by Western blot (Figure 8C–E). First, the expression level of caspase-8, a cysteine protease that initiates apoptotic signaling via the extrinsic pathway, was detected. Cleavage of pro-caspase-8 in the combined treatment was observed (Figure 8C). Our results showed a reduction of pro-caspase-9, the initiator caspase critical for the intrinsic pathway, concomitant with the appearance of a cleaved fragment at 18 kDa after the combined treatment. In line with the previous observation of increased caspase-3/7 activity for the combination treatment, we observed a strong cleavage of pro-caspase-3 and cleaved fragments of caspase-7 for the combined treatment (Figure 8D). Our evaluation of antiapoptotic Mcl-1 and Bcl-xL expression levels showed an increase of both in EE-84 (30 μM) and A-1210477 (10 μM) single treatments in K562 cells as well as in the combined treatment (Figure 8E).
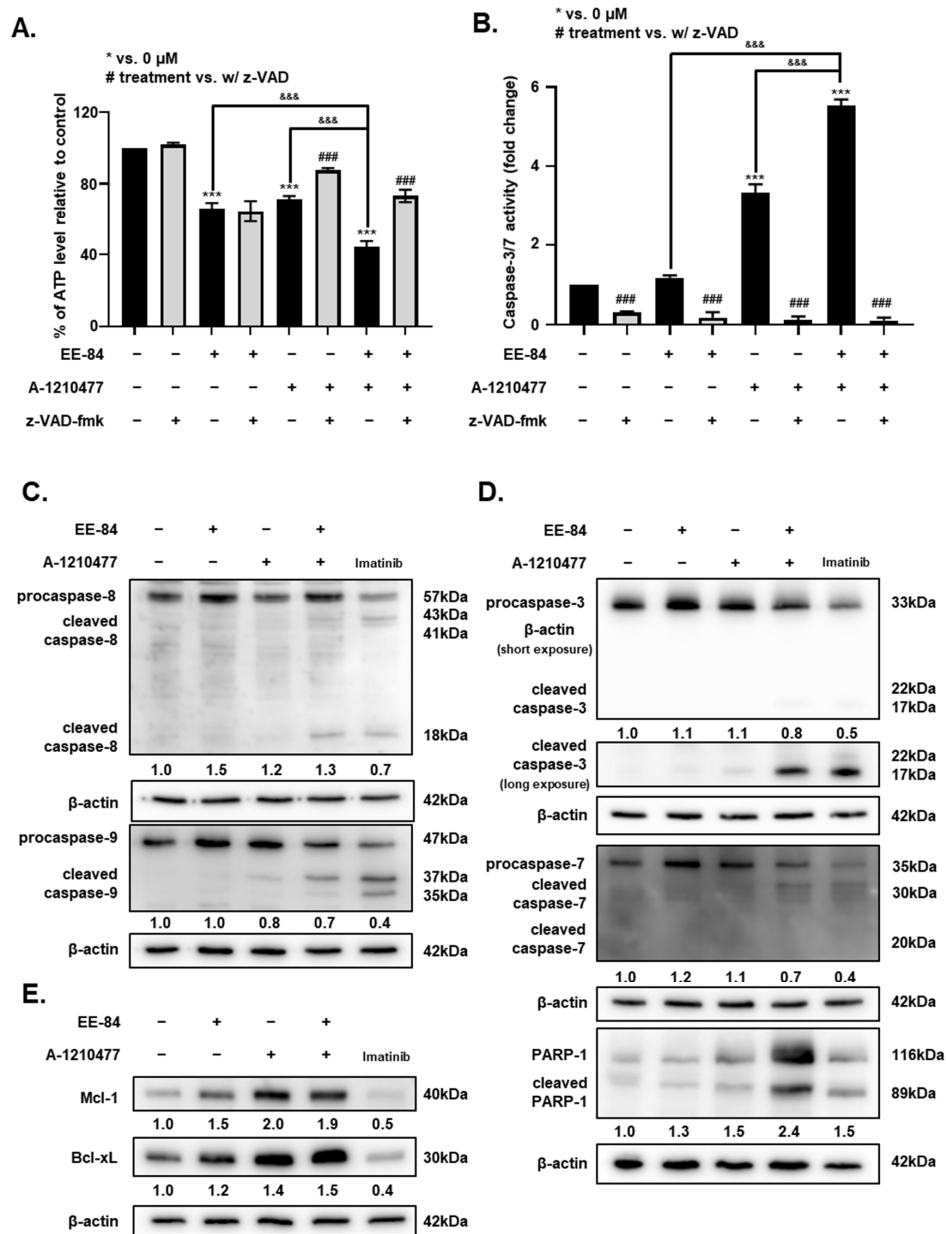
Figure 8. Caspase-dependent induction of apoptosis in K562 cells by EE-84 in synergism with the Mcl-1 inhibitor A-1210477. (**A**) K562 cell viability was determined by the measurement of cellular ATP content using the CellTiter-Glo assay. K562 cells were pretreated at the concentration of 50 μM z-VAD-fmk for 1 h before exposure to the compounds. (**B**) Effects of single or combination treatments of EE-84 and A-1210477 with or without z-VAD-fmk on caspase-3/7 activity in K562 cells. Three separate experiments were performed for both CellTiter-Glo and caspase-3/7 assays, and each condition was measured in triplicates. Values are the mean ± SD of three independent experiments. The asterisk indicates a value significantly different from the control. Statistical analysis was performed by one-way or two-way ANOVA, followed by Dunnett's multiple comparisons test (ATP assay, caspase-3/7 assay); *** $p < 0.001$ compared to controls; &&& $p < 0.001$ between indicated conditions; ### $p < 0.001$ compared to corresponding treatment without z-VAD-fmk. (**C**–**E**) Western blots showing expression levels of apoptosis-related proteins after single or combination treatments of EE-84 and A-1210477 in K562 cells. (**C**) Results of expression levels of initiator caspases, caspase-8 and -9; (**D**) expression levels of effector caspases, caspase-3 and -7, and PARP-1; (**E**) expression levels of antiapoptotic proteins Mcl-1 and Bcl-xL are displayed. Protein expression levels of procaspase-8, -9, -3, and -7 are quantified and expressed in fold changes relative to control. Protein expression levels of cleaved PARP-1, Mcl-1, and Bcl-xL are quantified and expressed in fold changes relative to control. The values represent the average of three independent experiments.

3. Discussion

Many products of marine organisms have been identified as modulators of cell death, exerting cytotoxic effects on cancer cells as activators of apoptosis, autophagy, or oncosis [19]. Currently, seven marine-based drugs have been approved, 23 compounds are undergoing phase I–III clinical trials, and thousands of compounds have been isolated from marine life and are undergoing preclinical studies [20]. Among these, four are used for cancer treatment: cytarabine (Cytosar-U®, Vitaris, Canonsburg, PA, USA), trabectedin (Yondelis®, PharmaMar, Colmenar Viejo, Madrid, Spain), eribulin mesylate (Halaven®, Eisai Inc., Tokyo, Japan) and the conjugated antibody brentuximab vedotin (Acentris®, Takeda Oncology, Cambridge, MA, USA) [21]. Cytosine arabinoside (cytarabine), originally isolated from the sponge *Cryptothethya crypa*, and now produced synthetically, is one of the most effective drugs to treat acute myeloid leukemia [21–23]. In addition, trabectedin, a marine metabolite of *Ecteinascidia turbinata*, is used for the treatment of soft tissue sarcoma [24]. However, despite the broad array of marine compounds clinically available or investigated, there is still an enormous library of natural products that remains untapped.

Aplysinopsins, a class of marine indole alkaloids, comprise two main distinct moieties—an indole and an imidazolidinone ring—and are isolated from a variety of marine organisms, including sponges [25], corals [26], anemone [27], and mollusks [28,29]. Aplysinopsins were first isolated by Kazlauskas et al., and initially identified as the major metabolite of eight Indo-Pacific sponge species of the genera *Thorecta* [12]. Since then, more aplysinopsin derivatives have been discovered and extracted from *Verongia spengeli*, *Dercitus* sp., *Smenospongia aurea*, *Verongular rigida*, *Dictyoceratida* sp., *Aplysinopsis reticulata*, *Aplysina* sp., *Hyrtios erecta*, and *Thorectandra* [28], among others. In line with the effort to identify new aplysinopsins with therapeutic potential, we report a set of synthetic aplysinopsin derivatives that possess anti-leukemic effects. In addition, aplysinopsin derivatives displayed a range of cytostatic effects, some inducing antiproliferating effects on myeloid leukemia cells more than others. We identified EE-84 as having the most potent antiproliferative effect in several chronic myeloid leukemia cell lines (K562, KBM5, MEG01, K562IR, and KBM5IR) as shown by trypan blue exclusion tests, CFAs, Hoechst/PI, and Annexin V/PI staining assays.

Identifying lead candidates from a library of compounds and characterizing their safety profiles by testing their toxicity in healthy models is essential in the drug discovery process. In addition, it helps predict clinical adverse effects in the future [28]. EE-84 showed differential toxicity in the noncancerous cell model, RPMI 1788, compared to K562, and was nontoxic to PBMCs. In the zebrafish model. EE-84 was also well-tolerated. The safe profile and drug-likeness of EE-84, supported by Lipinski's rule of five, warranted further investigation of this compound.

EE-84 induced morphological changes in K562 cells as shown by diff-Quik staining and TEM imaging. In parallel with the cytostatic effect, EE-84 triggered a significant increase in the cell size together with the appearance of mitochondrial damage after 48 h of treatment. Furthermore, evaluation of mitochondrial dysfunction by Agilent Seahorse XFp Cell Mito Stress test showed significant inhibition of mitochondrial function after 72 h of 30 μM treatment. Interestingly, EE-84-treated K562 cells displayed a senescent-like phenotype, suggesting an interplay between mitochondrial dysfunction and cellular senescence in the EE-84-induced antiproliferative effect.

Cellular senescence is one of the many defense mechanisms that cells undergo to combat extrinsic and/or intrinsic stresses by halting cell cycle progression. Drug-mediated cellular stress leading to senescence is often accompanied by senescence-associated secretory phenotype (SASP). Many studies revealed that in senescent cells, mitochondrial function is significantly affected [30]. For example, Galanos et al. showed perturbations in the mitochondrial morphology in p21-inducible precancerous and cancerous cellular models (Li-Fraumeni and Saos-2 cell lines), characterized by the enlargement of the mitochondria and the damaged morphology of cristae [31,32]. Mitochondria were elongated or branched, and the cristae were abnormally distributed or lost, suggesting a disturbance

of mitochondrial dynamics in the senescent cell. Wiley et al. also reported a distinct type of senescence associated with mitochondrial damage called "Mitochondrial Dysfunction Associated-Senescence" (MiDAS). They observed that mitochondrial dysfunction induces senescence and differs from the senescence caused by genotoxic or oncogenic stress by analyzing the secretome [33].

Senolytic compounds specifically induce apoptosis in senescent cells [34]. Dasatinib has been approved to treat CML as one of the second-generation tyrosine kinase inhibitors used in imatinib resistance and/or intolerance [35]. The senolytic drug combination of dasatinib and quercetin decreased senescent cells in human adipose tissue [36]. In addition, BH3 mimetic ABT-263 (Navitoclax) also induced apoptosis in mouse senescent bone marrow hematopoietic stem cells (HSCs) as a potent senolytic drug [37]. Hence, these studies support the idea that EE-84 triggered a senescent-like phenotype in response to mitochondrial dysfunction, autophagy, and prolonged ER stress as cellular metabolic alteration. In the present study, we showed that EE-84 induces a senescent-like phenotype. Interestingly, the combination of BH3 mimetic A-1210477 with EE-84 further triggers canonical apoptotic cell death in K562 and K562IR. We speculate that under these conditions, Mcl-1 inhibitor A-1210477 may act as a senolytic compound able to eradicate imatinib-sensitive and resistant CML cells. The effect of EE-84 as a single agent points at the ability of this compound to act as a general stress inducer. New effective combinatorial anticancer treatments also include stress inducers forcing cancer cells to rely more on a prosurvival factor. Targeting this specific protein promotes the eradication of cancer cells. Interestingly, some of the cases reported do involve prosurvival Bcl-2 family proteins. Dexamethasone, for example, is leading to Bcl-2 dependence and sensitization to venetoclax in multiple myeloma by altering the balance between pro- and antiapoptotic Bcl-2 protein members (increased Bim and decreased Mcl-1 vs. Bcl-2 upregulation), making Bcl-2 expression essential for survival [38]. Kapoor and colleagues report that CLL chronically resistant to ibrutinib (a Bruton tyrosine kinase (BTK) inhibitor) are sensitized to venetoclax partly also by a STAT3-mediated Bcl-2 upregulation in resistant CLL, implying a shift in the type of Bcl-2 family protein dependence [39]. At this level of investigation, we might speculate that EE-84 contributes to a similar scenario. Mcl-1 protein upregulation (or stabilization?) might signalize an increased reliance of CML cells on Mcl-1 as part of a stress response induced by EE-84. Further investigations will be required to elucidate any modulatory effects of EE-84 on the expression level of proapoptotic Bcl-2 proteins. In this view, EE-84 might be a compound to consider in combinatorial regimens.

Next, we investigated whether autophagy and ER stress occur concurrently with inhibition of proliferation by EE-84 in K562 cells. Accumulation of LC3-II, a standard marker for autophagosomes, was detected increasingly over time after 24, 48, and 72 h of EE-84 treatment, as seen in our Western blotting results. There was a significant increase in the formation of cytoplasmic vacuoles after 48 h EE-84 treatment at 30 μM, and this phenomenon was abrogated by a post-treatment with Baf-A1. Furthermore, 98.7% of K562 cells were viable after 48 h EE-84 treatment alone; however, the viability of K562 cells significantly decreased with Baf-A1 post-treatment, implying that EE-84 drives the K562 cells to undergo autophagy as a cell survival mechanism. ER stress was also activated by EE-84, given that sensor proteins of UPR, such as PERK and ATF6, and downstream effectors such as CHOP and ATF4 were upregulated to varying degrees. GRP78 has been initially characterized as a glucose-regulated protein [16]. Our Western blot results showed decreased levels of GRP78. These results are in line with data obtained by using the Seahorse glycolysis stress test. We observed reduced glycolysis levels, supporting the hypothesis of an impairment of the glycolytic function by EE-84 treatment in K562 and K562IR cells. Altogether, EE-84 induced autophagy, ER stress, and mitochondrial alterations as cell stress reactions, further leading to apoptosis. Overall, EE-84 plays a potential role in inhibiting CML cell activities via induction of cellular stress modalities.

The evasion of apoptotic cell death by cancer cells can impair responses to anticancer therapy. Prosurvival B-cell lymphoma 2 (BCL-2) proteins play a role of perpetrators in

this scenario because they prevent apoptosis by keeping the cell death effectors like BAX and BAK under control [40]. BH3 mimetics offer a solution to this as they are designed to inhibit antiapoptotic BCL2 family proteins, leading to BAX and BAK activation, and thus promoting apoptosis [41]. Mcl-1 became a popular therapeutic target because it is one of the most frequently amplified genes across all human cancers. Moreover, an increase in Mcl-1 expression is commonly associated with chemotherapy resistance [42]. This study evaluated the synergistic effect of EE-84, a cytostatic marine compound, with the Mcl-1 inhibitor A-1210477 against CML K562 and K562 imatinib-resistant cells. We showed that the cotreatment of the marine compound and the Mcl-1 inhibitor induced apoptotic cell death along with the activation of caspase activity. These results are in line with other studies in which BH3 mimetics like ABT199 showed synergism with cell stress inducers like cardiac glycosides [43,44] and coumarin derivatives [44].

In the present study, we investigated the preclinical use of aplysinopsins as anti-leukemic agents. Our results identify EE-84 as a potential drug candidate for CML as it possesses drug-like properties and is well-tolerated in healthy models in vitro and in vivo. Mechanistically, EE-84 induces antiproliferative effects associated with the complex interplay between mitochondrial dysfunction, a senescent-like phenotype, autophagy, and ER stress, potentially inducing a condition favorable for senolysis by synergizing with senolytic compounds. To potentiate the anti-leukemic effects of EE-84, we suggest the cotreatment of this aplysinopsin derivative with the BH3 mimetic A-1210477 in K562 and K562IR, as it significantly increases cell death of malignant cells. In conclusion, the combination of EE-84 with BH3 mimetics is efficient and highly synergistic. Future investigations will determine whether this combinatory approach can become a therapeutic opportunity against resistant forms of CML.

4. Materials and Methods

4.1. Chemistry

4.1.1. General Information

All reagents and solvents were of commercial grade. Melting points were determined on the digital melting point apparatus (Electro thermal 9100, Electro thermal Engineering Ltd., serial No. 8694, Rochford, UK) and are uncorrected. Elemental analyses were performed on a FlashSmart™ Elemental Analyzer (Thermo Scientific, Courtaboeuf, France) and were found within ±0.4% of the theoretical values.^{1}H and ^{13}C NMR spectra were measured with a Bruker Avance spectrometer (Bruker, Germany) at 400 and 101 MHz, respectively, using TMS as the internal standard. Hydrogen coupling patterns are described as (s) singlet, (d) doublet, (t) triplet, (q) quartet, and (m) multiplet. The chemical shifts were defined as parts per million (ppm) relative to the solvent peak. The reaction progress was checked by pre-coated TLC Silica gel 0.2 nm F254 nm [Fluka], visualized under UV lamp 254 and 365 nm. 2-Cyanoacetohydrazide [45]; N-benzyl indoles [46] methyl creatinine [47]; 5-methoxy indole-3-aldehyde [48] were prepared as reported. 1-(2-Amino-5-methyl-4,5,6,7-tetrahydrobenzo[b]thiophen-3-yl)ethan-1-one [49] was provided by Ahmed B. Abdelwahab, Ph.D., UMR CNRS 7565 SRSMC, Université de Lorraine, 57070 Metz, France.

4.1.2. General Procedure for the Preparation of EE-31, EE-80, EE-84, EE-92

To a solution at 0 °C of oxalyl chloride (0.44 mL, 5.1 mmol) in dry ethyl ether (25 mL) was added dropwise a solution of indole (4.14 mmol) in dry ethyl ether (5 mL). The resulting solution was refluxed for 2 h. After removing the solvent under vacuo, the residue was dissolved in dry tetrahydrofuran (20 mL) and cooled to 0 °C. To the THF solution was added slowly the amine (9.73 mmol) in dry tetrahydrofuran (20 mL). After complete addition, 1 mL of triethylamine was added, and the reaction was left to stir overnight. The precipitate obtained was filtered off, washed several times with water, dried, and recrystallized from acetone.

2-(1-Benzyl-1H-Indol-3-yl)-N′-(2-Cyanoacetyl)-2-Oxoacetohydrazide EE-31

Yield 0.45g, 86%; mp 264–6 °C; ^{1}H NMR (400 MHz, DMSO) δ: 10.63 (s, 1H), 8.90 (s, 1H), 8.26 (s, 1H), 7.72–7.50 (m, 5H), 7.41–7.21 (m, 4H), 5.46 (s, 2H), 3.83 (s, 2H); 13C NMR (101 MHz, DMSO) δ: 162.16, 141.47, 136.79, 136.70, 129.14, 128.97, 128.56, 128.26, 128.01, 127.73, 127.65, 127.29, 126.98, 124.17, 123.56, 122.53, 121.92, 116.04, 112.14, 111.95, 50.28, 24.10; Anal. Calcd for $C_{20}H_{16}N_4O_3$ (360.37): C, 66.66; H, 4.48; N, 15.55; found: C, 66.87; H, 4.50; N, 15.42.

2-(1-Benzyl-5-Methoxy-1H-Indol-3-yl)-N′-(2-Cyanoacetyl)-2-Oxoacetohydrazide EE-80

Yield (0.31g, 63%); mp 199–201 °C; ^{1}H NMR (400 MHz, DMSO) δ: 10.62 (s, 1H), 8.78 (s, 1H), 7.76 (s, 1H), 7.57–7.43 (d, H), 7.41–7.20 (m, 5H), 7.06–6.77 (m, 2H), 5.44 (s, 2H), 3.87 (m, 3H), 3.33 (s, 2H); ^{13}C NMR (101 MHz, DMSO) δ 161.34, 162.32, 156.47, 136.51, 131.22, 128.74, 127.83, 127.60, 127.33, 115.52, 113.07, 112.52, 103.72, 55.37, 50.06, 23.80; Anal. Calcd for $C_{21}H_{18}N_4O_4$ (390.40): C, 64.61; H, 4.65; N, 14.35; found: C, 64.55; H, 4.70; N, 14.32.

(N-(3-Acetyl-4,5,6,7-Tetrahydro-5-Methylbenzo[b]Thiophen-2-yl)-2-(1-Benzyl-5-Methoxy-1H-Indol-3-yl)-2-Oxoacetamide EE-84

Yield (0.38g, 61%); mp 165–7 °C; ^{1}H NMR (400 MHz, CDCl$_3$) δ: 13.58 (s, 1H), 9.07 (s, 1H), 8.08 (d, *J* = 2.5 Hz, 1H), 7.35–6.90 (m, 8H), 5.38 (s, 2H), 3.92 (d, *J* = 6.4 Hz, 3H), 2.82–2.80 (dd, *J* = 16.1, 5.0 Hz, 1H), 2.58–2.55 (m, 2H), 2.41 (s, 3H), 1.91–1.87 (m, 2H), 1.15 (d, *J* = 6.4 Hz, 2H), 1.10 (d, *J* = 6.6 Hz,3H); ^{13}C NMR (101 MHz, CDCl$_3$) δ: 196.38, 194.06, 164.12, 157.30, 140.94, 135.40, 131.26, 130.59, 130.42, 129.06, 128.98, 128.29, 128.24, 126.91, 123.08, 117.26, 115.78, 114.52, 111.48, 104.33, 55.81, 51.54, 36.56, 35.96, 31.01, 30.65, 29.25, 24.52, 21.76; Anal. Calcd for $C_{29}H_{28}N_2O_4S$ (500.61): C, 69.58; H, 5.64; N, 5.60; S, 6.40; found: C, 69.60; H, 5.56; N, 5.60; S, 6.48.

N′-(2-Cyanoacetyl)-2-(1-(2,4-Dichlorobenzyl)-5-Methoxy-1H-Indol-3-yl)-2-Oxoacetohydrazide EE-92

Yield (0.25g, 56%); mp 242–4 °C; 1H NMR (400 MHz, DMSO) δ: 10.74 (s, 1H), 10.39 (s, 1H), 8.70 (s, 1H), 7.75 (dd, *J* = 17.6, 2.3 Hz, 2H), 7.58–7.26 (m, 2H), 7.09–6.83 (m, 2H), 5.65 (s, 2H), 3.82 (s, 3H), 3.34 (s, 2H); 13C NMR (101 MHz, DMSO) δ: 180.68, 161.35, 156.58, 140.97, 133.49, 133.29, 132.90, 131.21, 130.50, 129.22, 127.88, 113.29, 112.27, 111.62, 103.79, 55.39, 47.52, 23.80; Anal. Calcd for C21H16Cl2N4O4 (459.28): C, 54.92; H, 3.51; Cl, 15.44; N, 12.20; found: C, 54.93; H, 3.46; Cl, 15.54; N, 12.33.

4.1.3. General Procedure for the Preparation of EE-115

1,3-Dimethyl creatinine (2.8 g, 22.7 mmol) and indole-3-aldehydes (22.7 mmol) were heated under reflux in piperidine (30 mL) for 4 h. After cooling, the reaction mixture was poured into water (200 mL) and then stirred for 30 min. The precipitate was filtered, washed several times with water, air dried and crystallized from methanol.

(Z)-5-((1H-Indol-3-yl)Methylene)-1,3-Dimethylimidazolidine-2,4-Dione (Aplysinopsin) EE-115 [50]

Yield 80%, mp 236–8 °C (reported mp 236 °C); ^{1}H NMR (400 MHz, CDCl$_3$) δ: 8.87 (d, *J* = 2.7 Hz, 1H), 8.54 (s, 1H), 7.85–7.66 (m, 1H), 7.45 (dd, *J* = 6.7, 1.4 Hz, 1H), 7.33–7.18 (m, 3H), 6.42 (s, 1H), 3.34 (s, 3H), 3.23 (s, 3H).

4.2. *Cell Lines and Cell Cultures*

The human chronic myeloid leukemia K562 (ATCC, CCL-243, Manassas, VA, USA), MEG01 (ATCC, CRL-2021, Manassas, VA, USA), and the normal B lymphocyte RPMI 1788 cell lines (KCLB, 10156, Seoul, Korea) were cultured in Roswell Park Memorial Institute (RPMI) 1640 medium (Lonza, Basel, Switzerland), supplemented with 10% heat-inactivated fetal bovine serum (FBS) (Biowest, Riverside, CA, USA) and 1% penicillin-streptomycin solution (100×) (GenDEPOT, Katy, TX, USA). KBM-5 cells were kindly donated by Dr. Bharat B. Aggarwal. Imatinib-resistant KBM5 cells (KBM5R) cells were obtained by sequentially increasing the concentration of imatinib from 0.25 to 1 μM imatinib in IMDM media

supplemented with 10% (*v/v*) fetal calf serum and 1% (*v/v*) antibiotic–antimycotics [51]. Imatinib-resistant K562 (K562IR) cells were a gift of the Catholic University of Seoul and cultured in RPMI 1640 medium with 25 mM HEPES (Lonza) supplemented with 10% (*v/v*) FCS and 1% (*v/v*) antibiotic–antimycotics. Both resistant cell types were cultured with 1 μM of imatinib and washed three times before each experiment. Cells were maintained at 37 °C and 5% of CO_2 in a humified atmosphere. Mycoplasma detection by Mycoalert™ (Lonza) was performed every 30 days, and cells were used within three months after thawing.

Peripheral blood mononuclear cells (PBMCs) were isolated by density gradient centrifugation using Ficoll-Hypaque (GE Healthcare, Roosendaal, The Netherlands) from freshly collected buffy coats as previously described [51], obtained from healthy adult human volunteers (Red Cross, Luxembourg City, Luxembourg) after ethical approval as well as written informed consent from each volunteer. After isolation, cells were incubated overnight at 2×10^6 cells/mL in RPMI 1640 (supplemented with 1% antibiotic–antimycotic and 10% FCS (BioWhittaker, Verviers, Belgium) at 37 °C and 5% CO_2 in a humidified atmosphere. The day after, cell concentration was adjusted at 1×10^6 cells/mL using the same fresh complete medium and then treated as indicated.

4.3. Compounds

Mcl-1 inhibitor, A-1210477 (S7790, Selleckchem, Seoul, Korea) was used in single and combination treatments. Etoposide (E1383, Sigma-Aldrich, Seoul, Korea), Imatinib (SML 1027, Sigma-Aldrich, St. Louis, MO, USA), and Celecoxib (PZ0008, Sigma-Aldrich, Seoul, Korea) were used as positive controls. Caspase inhibitor 1 (z-VAD-fmk, 187389-52-2, Calbiochem, Seoul, Korea) served to inhibit caspase-dependent apoptosis.

4.4. Cell Proliferation and Viability

Cell proliferation and viability were assessed by the trypan blue exclusion method (Lonza), and viable cells were counted using a hematocytometer (Marienfeld, Lauda-Königshofen, Germany). Differential toxicity was calculated by comparing the viability of RPMI 1788 cells to the viability of cancer cells (normal/cancer cells). The difference in viability was expressed in terms of fold change.

4.5. Colony Formation Assay

For 48 h pretreatment of EE-84 colony formation assays, approximately 3×10^5 cells were seeded in each well of a 24-well plate, treated with EE-84 at indicated concentrations, and incubated at 37 °C and 5% of CO_2 in a humidified atmosphere for 48 h. After 48 h, 1000 cells were counted and grown in a semisolid methylcellulose medium (Methocult H4230, StemCell Technologies Inc., Vancouver, BC, Canada) supplemented with 10% FBS. Colonies were detected after 10 days of culture by adding 1 mg/mL of 3-(4,5-dimethylthiazol-2-yl)-2,5-diphenyltetrazolium bromide (MTT) reagent (Sigma-Aldrich) and were analyzed by Image J 1.8.0 software (U.S. National Institute of Health, Bethesda, MD, USA).

4.6. Quantification of Apoptosis and Necrosis

The percentage of apoptotic cells was quantified as the fraction of cells showing fragmented nuclei, as assessed by fluorescence microscopy (Nikon, Tokyo, Japan) after staining with Hoechst 33342 (Sigma-Aldrich) and propidium iodide (Sigma-Aldrich). In addition, apoptosis was confirmed by Annexin V APC (Biolegend, 640919)/propidium iodide (BD Biosciences, 556547) staining and fluorescence-activated cell sorter (FACS) analysis according to the manufacturer protocol (BD Biosciences, 556547).

4.7. In Silico Drug Likeliness Properties

Lipinski's 'rule of five' for drug likeliness properties was evaluated using the SCFBio website (http://www.scfbio-iitd.res.in/).

4.8. Zebrafish Toxicity

For toxicity assays, embryos were treated with 0.003% phenylthiourea (PTU) 14 h before the assay to remove pigmentation. Then, 2 h before the assay, the embryo's shell was eliminated and then treated for up to 24 h with aplysinopsin compounds at indicated concentrations in 24-well plates. Viability and abnormal development were assessed after 24 h of treatment under light microscopy (Carl Zeiss Stereomicroscope DV4, Seoul, Korea). Pictures were taken by fixing embryos onto a glass slide with 3% methylcellulose (Sigma-Aldrich).

4.9. Cell Cycle Analysis

Cells were collected and fixed in 70% ethanol. DNA was stained with propidium iodide (PI) solution (1 μg/mL, Sigma-Aldrich, St. Louis, MO, USA) in 1XPBS (Biosesang, Seongnam, Korea) for 30 min at 37 °C, supplemented with RNase A (100 μg/mL, Roche, Basel, Switzerland). Samples were analyzed by flow cytometry using the FACSCalibur^{TM} system, Becton Dickinson (BD) Biosciences (San Jose, CA, USA). Data were recorded statistically (10,000 events/sample) using the Cell Quest software (BD Biosciences) and analyzed using Flow-Jo 8.8.5 software (Tree Star, Inc., Ashland, OR, USA).

4.10. Cell Morphology/Wright-Giemsa Staining

Diff Quik staining was used to analyze the morphological features of compound-treated cells. Approximately 3×10^5 cells were seeded in each well of a 24-well plate and treated with EE-84 at the indicated concentrations for the indicated time. Cells were then spun onto a microscope glass slide for 5 min at $500 \times g$ using a cytopad with caps (Elitech Group Inc., Puteaux, France). Cells were fixed, air-dried, and then stained with the Diff-Quik staining kit (Sysmex, Kobe, Japan). The stained cells were examined, and images were captured with an inverted microscope (Nikon Eclipse Ti2).

4.11. SA-β-Gal Assay

The senescence-associated (SA)-β-Gal activity was measured as previously reported [52]. K562 cells treated with 80 nM doxorubicin 72 h were used as a positive control for senescence induction.

4.12. Analysis of Cell Size and Complexity (Granularity)

Flow cytometry acquisitions of FSC-H (forward) vs. SSC-H (size) were performed as a method to monitor the cell size and granularity (cell complexity) in untreated vs. EE-84-treated K562 (FACSCalibur^{TM}; BD Biosciences). Data (10,000 events) were recorded using the Cellquest Pro software (BD Biosciences) and further analyzed using FlowJo software (Treestar, Ashland, OR, USA).

4.13. Analysis of Mitochondrial Membrane Potential (MMP) Levels

To monitor mitochondrial membrane potential (MMP), cells were incubated at 37 °C for 30 min with 50 nM MitoTracker Red CMXRos (all from Molecular Probes, Invitrogen, Grand Island, NY, USA) and then analyzed by flow cytometry. Data were recorded statistically (10,000 events/sample) using the CellQuest Pro software. Data were analyzed using the Flow-Jo 8.8.7 software, and results were expressed as cells with MMP loss (%).

4.14. Transmission Electron Microscopy (TEM)

Cells were pelleted and fixed in 2.5% glutaraldehyde (Electron Microscopy Sciences, Hatfield, PA, USA) diluted in 0.1 M sodium cacodylate buffer, pH 7.2 (Electron Microscopy Sciences) overnight. Cells were then rinsed twice with sodium cacodylate buffer, postfixed for 2 h in 2% osmium tetroxide at room temperature, washed with distilled water, and stained with 0.5% uranyl acetate at 4 °C overnight. Samples were then dehydrated in successive ethanol washes, followed by infiltration of 1 (100% ethanol):1 (Spurr's resin). Samples were kept overnight embedded in 100% Spurr's resin, mounted in molds, and

left to polymerize in an oven at 56 °C for 48 h. Ultrathin sections (70–90 nm) were cut with an ultramicrotome, EM UC7 (Leica Microsystems Ltd., Seoul, Korea). Sections were stained with uranyl acetate and lead citrate and subsequently viewed using a JEM1010 transmission electron microscope (JEOL Korea Ltd., Seoul, Korea).

4.15. Determination of the Oxygen Consumption Rate and Glycolysis Stress

The oxygen consumption rate (OCR) was measured using a Seahorse XFp Cell Mito Stress Assay (#103010-100, Agilent Technologies, Seoul, Korea) ran on a Seahorse XFp analyzer (Agilent Technologies, Seoul, Korea) according to the manufacturer's instructions. Briefly, cells were seeded at 30,000 cells per well and treated with EE-84 for 48 h in 175 μL medium. Before measurements, plates were equilibrated in a CO_2-free incubator at 37 °C for 1 h. The analysis was performed using 1.5 μM oligomycin, 0.5 μM carbonyl cyanide-4-(trifluoromethoxy)phenylhydrazone (FCCP), and 1 μM rotenone/antimycin A as indicated. Data were analyzed using the Seahorse XF Cell Mito Stress Test report generator software (Agilent). The extracellular acidification rate (ECAR) was measured in response to the sequential injection of 10 mM glucose, 2 μM oligomycin (H+-ATP-synthase inhibitor), and 50 mM 2-deoxy-d-glucose (2DG) (hexokinase inhibitor) to detect non-glycolytic acidification, glycolysis, maximal glycolytic capacity, and glycolytic reserve using a Seahorse XFp analyzer with a Glycolysis Stress Test kit (Agilent, Santa Clara, CA, USA).

4.16. Measurement of Intracellular ATP Content

To quantify metabolically active cells, intracellular ATP levels were measured by CellTiter-Glo Luminescent Cell Viability Assay (Promega, Cosmogenetech, Seoul, Korea) following the manufacturer's protocol.

4.17. Measurement of Caspase-3/7 Activity

According to the manufacturer's instructions, the activation of caspase-3/7 was measured using the Caspase-Glo 3/7 Assay (Promega, Madison, WI, USA). The caspase-3/7 reagent was added to the sample volume at a 1:1 ratio, and the cells were incubated for 1 h at room temperature. The luminescence of triplicate samples was measured using a microplate reader.

4.18. Whole-Cell Extracts and Western Blotting

For the preparation of whole-cell extracts, cells were harvested, washed in cold 1xPBS, and lysed in Mammalian Protein Extraction Reagent (M-PER™, Thermo Fisher, Waltham, MA, USA) supplemented with a $1\times$ protease inhibitor cocktail (Complete, EDTA-free, Roche, Basel, Switzerland) according to the manufacturer's instructions. Protein concentration was measured using the Bradford assay. Proteins were aliquoted and stored at −80 °C. Afterward, proteins were subjected to sodium dodecyl sulfate (SDS)–polyacrylamide gel electrophoresis (PAGE) and transferred to PVDF membranes (GE Healthcare, Little Chalfont, UK). Membranes were incubated with selected primary antibodies: anti-caspase-7 (9494S), anti-caspase-9 (9502S), anti-caspase-8 (9746), anti-Mcl-1 (4572S), anti-LC3B (2775), ATF4 (11815), ATF6 (65880), Bip/GRP78 (C50B12), CHOP (L63F7), eIF2α (9722) and PERK (3192) from Cell Signaling (Danvers, MA, USA), anti-caspase-3 (sc-56053) and anti-PARP-1 (sc-53643) from Santa Cruz Biotechnology (Dallas, TX, USA), anti-Bcl-xL (610212) from BD Pharmingen (San Jose, CA, USA), eIF2a (Phospho-Ser51) (11279) from Signalway Antibody Co. (College Park, MD, USA) and anti-β-actin (5441) from Sigma Aldrich (St. Louis, MO, USA). Blots were probed in PBS-T containing the appropriate blocking agent (5% milk or 5% BSA) for 1 h. Membranes were prehybridized overnight with the indicated primary antibodies. After washing, blots were incubated with species-appropriate HRP-conjugated secondary antibody (Santa Cruz) in PBS-T containing 5% milk. Proteins of interest were detected with ECL Plus Western blotting Detection System reagent (GE Healthcare) using ImageQuant LAS 4000 mini system (GE Healthcare).

4.19. Statistical Analysis

Data are expressed as the mean $\pm$ SD and significance was estimated by using one-way or two-way ANOVA (analysis of variance) followed by either Dunnett's multiple comparison test or Sidak's multiple comparison test, unless otherwise stated, using Prism 8 software, GraphPad Software (La Jolla, CA, USA). *p*-values were considered statistically significant when $p < 0.05$. Legends are represented as follows: * $p < 0.05$, ** $p < 0.01$, *** $p < 0.001$.

5. Conclusions

Through the screening of several aplysinopsin analogs, we selected EE-84 as an interesting anti-leukemic agent. EE-84 exhibited a safety profile as it had minimal impact on healthy models in vitro and in vivo. We also found that the treatment of K562 with EE-84 induced an antiproliferative effect concomitant with autophagy and ER stress induction as well as senescence. In addition, mitochondrial dysfunction was observed in line with altered K562 cell morphology after EE-84 treatment. Treatment of EE-84 combined with the BH3 mimetic A-1210477 (specific for Mcl-1) potentialized apoptotic cell death. We suggest this cotreatment as a promising preclinical approach to therapeutic failure, specifically in resistant CML.

Conflicts of Interest: The authors declare no conflict of interest.

Abbreviations

AML	acute myeloid leukemia
Bcr-Abl	breakpoint cluster region-Abelson
BH	Bcl-2 homology domain
BSA	bovine serum albumin
CCyR	complete cytogenetic response
CFA	colony formation assay
CML	chronic myeloid leukemia
DMSO	dimethyl sulfoxide
FBS	fetal bovine serum
FDA	food and drug administration
FLT3	FMS-like tyrosine kinase 3
GI	growth inhibition
HPF	hours post fertilization
IC	inhibitory concentration
ITD	internal tandem duplication
LogP	octanol–water partition coefficient
MPER	mammalian protein extraction reagent
Mcl-1	myeloid cell leukemia 1
MMP	mitochondrial membrane potential
MTT	3-(4,5-dimethylthiazol-2-1)-2,5,-diphenyltetrazolium bromide
PARP-1	poly(ADP-ribose)polymerase
PBMC	peripheral blood mononuclear cell
PBS	phosphate buffered saline
PI	propidium iodide
PMSF	phenylmethylsulphonyl fluoride
PTU	phenylthiourea
RPMI	Roswell Park Memorial Institute
SA	surface area
SD	standard deviation
SDS-PAGE	sodium dodecyl sulfate polyacrylamide gel electrophoresis
TEM	transmission electron microscopy
TKD	tyrosine kinase domain
UPR	unfolded protein response

References

1. Kang, Z.-J.; Liu, Y.-F.; Xu, L.-Z.; Long, Z.-J.; Huang, D.; Yang, Y.; Liu, B.; Feng, J.-X.; Pan, Y.-J.; Yan, J.-S.; et al. The Philadelphia chromosome in leukemogenesis. *Chin. J. Cancer* **2016**, *35*, 1–15. [CrossRef] [PubMed]
2. Cheng, Y.-C.; Chang, J.-M.; Chen, C.-A.; Chen, H.-C. Autophagy modulates endoplasmic reticulum stress-induced cell death in podocytes: A protective role. *Exp. Biol. Med.* **2015**, *240*, 467–476. [CrossRef] [PubMed]
3. Bhamidipati, P.K.; Kantarjian, H.; Cortes, J.; Cornelison, A.M.; Jabbour, E. Management of imatinib-resistant patients with chronic myeloid leukemia. *Ther. Adv. Hematol.* **2012**, *4*, 103–117. [CrossRef] [PubMed]
4. Liu, Y.; Gong, W.; Yang, Z.Y.; Zhou, X.S.; Gong, C.; Zhang, T.R.; Wei, X.; Ma, D.; Ye, F.; Gao, Q.L. Quercetin induces protective autophagy and apoptosis through ER stress via the p-STAT3/Bcl-2 axis in ovarian cancer. *Apoptosis* **2017**, *22*, 544–557. [CrossRef]
5. Hetz, C.; Chevet, E.; Harding, H.P. Targeting the unfolded protein response in disease. *Nat. Rev. Drug Discov.* **2013**, *12*, 703–719. [CrossRef]
6. Kim, I; Xu, W.; Reed, J.C. Cell death and endoplasmic reticulum stress: Disease relevance and therapeutic opportunities. *Nat. Rev. Drug Discov.* **2008**, *7*, 1013–1030. [CrossRef]
7. Murrow, L.; Debnath, J. Autophagy as a Stress-Response and Quality-Control Mechanism: Implications for Cell Injury and Human Disease. *Annu. Rev. Pathol. Mech. Dis.* **2013**, *8*, 105–137. [CrossRef]
8. Yin, H.; Zhao, L.; Jiang, X.; Li, S.; Huo, H.; Chen, H. DEV induce autophagy via the endoplasmic reticulum stress related unfolded protein response. *PLoS ONE* **2017**, *12*, e0189704. [CrossRef] [PubMed]
9. Molina, P.; Almendros, P.; Fresneda, P.M. Iminophosphorane-Mediated Imidazole Ring Formation—A New and General Entry to Aplysinopsin-Type Alkaloids of Marine Origin. *Tetrahedron* **1994**, *50*, 2241–2254. [CrossRef]

10. Segraves, N.L.; Crews, P. Investigation of brominated tryptophan alkaloids from two thorectidae sponges: Thorectandra and Smenospongia. *J. Nat. Prod.* **2005**, *68*, 1484–1488. [CrossRef]

11. Newman, D.J.; Cragg, G.M. Natural Products as Sources of New Drugs from 1981 to 2014. *J. Nat. Prod.* **2016**, *79*, 629–661. [CrossRef]

12. Kazlauskas, R.; Murphy, P.T.; Quinn, R.J.; Wells, R.J. Aplysinopsin, a new tryptophan derivative from a sponge. *Tetrahedron Lett.* **1977**, *18*, 61–64. [CrossRef]

13. Lipinski, C.A.; Lombardo, F.; Dominy, B.W.; Feeney, P.J. Experimental and computational approaches to estimate solubility and permeability in drug discovery and development settings. *Adv. Drug Deliv. Rev.* **2001**, *46*, 3–26. [CrossRef]

14. Radogna, F.; Dicato, M.; Diederich, M. Cancer-type-specific crosstalk between autophagy, necroptosis and apoptosis as a pharmacological target. *Biochem. Pharmacol.* **2015**, *94*, 1–11. [CrossRef]

15. Yoshida, H. ER stress and diseases. *FEBS J.* **2007**, *274*, 630–658. [CrossRef]

16. Li, Z.; Wang, Y.; Newton, I.P.; Zhang, L.; Ji, P.; Li, Z. GRP78 is implicated in the modulation of tumor aerobic glycolysis by promoting autophagic degradation of IKKbeta. *Cell Signal.* **2015**, *27*, 1237–1245. [CrossRef]

17. Jiang, C.C.; Lucas, K.; Avery-Kiejda, K.A.; Wade, M.; Debock, C.E.; Thorne, R.F.; Allen, J.; Hersey, P.; Zhang, X.D. Up-regulation of Mcl-1 Is Critical for Survival of Human Melanoma Cells upon Endoplasmic Reticulum Stress. *Cancer Res.* **2008**, *68*, 6708–6717. [CrossRef]

18. Hu, J.; Dang, N.; Menu, E.; De Bryune, E.; Xu, D.; Van Camp, B.; Van Valckenborgh, E.; Vanderkerken, K. Activation of ATF4 mediates unwanted Mcl-1 accumulation by proteasome inhibition. *Blood* **2012**, *119*, 826–837. [CrossRef]

19. Folmer, F.; Jaspars, M.; Dicato, M.; Diederich, M. Marine cytotoxins: Callers for the various dances of death. *Gastroenterol. Hepatol.* **2009**, *2*, S34–S50.

20. Malve, H. Exploring the ocean for new drug developments: Marine pharmacology. *J. Pharm. Bioallied Sci.* **2016**, *8*, 83–91. [CrossRef]

21. Jimenez, P.C.; Wilke, D.V.; Costa-Lotufo, L.V. Marine drugs for cancer: Surfacing biotechnological innovations from the oceans. *Clincs* **2018**, *73*, e482s. [CrossRef]

22. Roberts, W.K.; Dekker, C.A. A convenient synthesis of arabinosylcytosine (cytosine arabinoside). *J. Org. Chem.* **1967**, *32*, 816–817. [CrossRef] [PubMed]

23. Bergmann, W.; Feeney, R.J. Contributions to the Study of Marine Products. Xxxii. The Nucleosides of Sponges. I.1. *J. Org. Chem.* **2002**, *16*, 981–987. [CrossRef]

24. Mayer, A.M.; Glaser, K.B.; Cuevas, C.; Jacobs, R.S.; Kem, W.; Little, R.D.; McIntosh, J.M.; Newman, D.J.; Potts, B.C.; Shuster, D.E. The odyssey of marine pharmaceuticals: A current pipeline perspective. *Trends Pharmacol. Sci.* **2010**, *31*, 255–265. [CrossRef] [PubMed]

25. Hollenbeak, K.H.; Schmitz, F.J. Aplysinopsin: Antineoplastic tryptophan derivative from the marine sponge Verongia spengelii. *Lloydia* **1977**, *40*, 479–481.

26. Murata, M.; Miyagawa-Kohshima, K.; Nakanishi, K.; Naya, Y. Characterization of Compounds That Induce Symbiosis between Sea Anemone and Anemone Fish. *Science* **1986**, *234*, 585–587. [CrossRef]

27. Okuda, R.K.; Klein, D.; Kinnel, R.B.; Li, M.; Scheuer, P.J. Marine natural products: The past twenty years and beyond. *Pure Appl. Chem.* **1982**, *54*, 1907–1914. [CrossRef]

28. Bialonska, D.; Zjawiony, J.K. Aplysinopsins-Marine Indole Alkaloids: Chemistry, Bioactivity and Ecological Significance. *Mar. Drugs* **2009**, *7*, 166–183. [CrossRef]

29. Hu, J.F.; Schetz, J.A.; Kelly, M.; Peng, J.N.; Ang, K.K.; Flotow, H.; Leong, C.Y.; Ng, S.B.; Buss, A.D.; Wilkins, S.P.; et al. New antiinfective and human 5-HT2 receptor binding natural and semisynthetic compounds from the Jamaican sponge Smenospongia aurea. *J. Nat. Prod.* **2002**, *65*, 476–480. [CrossRef]

30. Yoon, Y.-S.; Yoon, D.-S.; Lim, I.K.; Yoon, S.-H.; Chung, H.-Y.; Rojo, M.; Malka, F.; Jou, M.-J.; Martinou, J.-C.; Yoon, G. Formation of elongated giant mitochondria in DFO-induced cellular senescence: Involvement of enhanced fusion process through modulation of Fis1. *J. Cell. Physiol.* **2006**, *209*, 468–480. [CrossRef]

31. Galanos, P.; Vougas, K.; Walter, D.; Polyzos, A.; Maya-Mendoza, A.; Haagensen, E.J.; Kokkalis, A.; Roumelioti, F.-M.; Gagos, S.; Tzetis, M.; et al. Chronic p53-independent p21 expression causes genomic instability by deregulating replication licensing. *Nat. Cell Biol.* **2016**, *18*, 777–789. [CrossRef] [PubMed]

32. Galanos, P.; Pappas, G.; Polyzos, A.; Kotsinas, A.; Svolaki, I.; Giakoumakis, N.N.; Glytsou, C.; Pateras, I.S.; Swain, U.; Souliotis, V.L.; et al. Mutational signatures reveal the role of RAD52 in p53-independent p21-driven genomic instability. *Genome Biol.* **2018**, *19*, 1–18. [CrossRef]

33. Wiley, C.D.; Velarde, M.C.; Lecot, P.; Liu, S.; Sarnoski, E.A.; Freund, A.; Shirakawa, K.; Lim, H.W.; Davis, S.S.; Ramanathan, A.; et al. Mitochondrial Dysfunction Induces Senescence with a Distinct Secretory Phenotype. *Cell Metab.* **2016**, *23*, 303–314. [CrossRef] [PubMed]

34. Petrova, N.V.; Velichko, A.K.; Razin, S.V.; Kantidze, O.L. Small molecule compounds that induce cellular senescence. *Aging Cell* **2016**, *15*, 999–1017. [CrossRef]

35. Keskin, D.; Sadri, S.; Eskazan, A.E. Dasatinib for the treatment of chronic myeloid leukemia: Patient selection and special considerations. *Drug Des. Dev. Ther.* **2016**, *10*, 3355–3361. [CrossRef]

36. Hickson, L.J.; Prata, L.G.L.; Bobart, S.A.; Evans, T.K.; Giorgadze, N.; Hashmi, S.K.; Herrmann, S.M.; Jensen, M.D.; Jia, Q.; Jordan, K.L.; et al. Senolytics decrease senescent cells in humans: Preliminary report from a clinical trial of Dasatinib plus Quercetin in individuals with diabetic kidney disease. *EBioMedicine* **2019**, *47*, 446–456. [CrossRef] [PubMed]

37. Chang, J.; Wang, Y.; Shao, L.; Laberge, R.-M.; DeMaria, M.; Campisi, J.; Janakiraman, K.; Sharpless, N.E.; Ding, S.; Feng, W.; et al. Clearance of senescent cells by ABT263 rejuvenates aged hematopoietic stem cells in mice. *Nat. Med.* **2016**, *22*, 78–83. [CrossRef]

38. Matulis, S.M.; Gupta, V.A.; Nooka, A.K.; Von Hollen, H.; Kaufman, J.L.; Lonial, S.; Boise, L.H. Dexamethasone treatment promotes Bcl-2 dependence in multiple myeloma resulting in sensitivity to venetoclax. *Leukemia* **2016**, *30*, 1086–1093. [CrossRef]

39. Kapoor, I.; Bodo, J.; Hill, B.T.; Hsi, E.D.; Almasan, A. Targeting BCL-2 in B-cell malignances and overcoming therapeutic resistance. *Cell Death Dis.* **2020**, *11*, 1–11. [CrossRef]

40. Giam, M.; Huang, D.C.S.; Bouillet, P. BH3-only proteins and their roles in programmed cell death. *Oncogene* **2008**, *27*, S128–S136. [CrossRef]

41. Ni Chonghaile, T.; Letai, A. Mimicking the BH3 domain to kill cancer cells. *Oncogene* **2008**, *27*, S149–S157. [CrossRef]

42. Chonghaile, T.N. BH3 mimetics: Weapons of cancer cell destruction. *Sci. Transl. Med.* **2019**, *11*, eaaw5311. [CrossRef]

43. Cerella, C.; Gaigneaux, A.; Mazumder, A.; Lee, J.-Y.; Saland, E.; Radogna, F.; Farge, T.; Vergez, F.; Récher, C.; Sarry, J.-E.; et al. Bcl-2 protein family expression pattern determines synergistic pro-apoptotic effects of BH3 mimetics with hemisynthetic cardiac glycoside UNBS1450 in acute myeloid leukemia. *Leukemia* **2016**, *31*, 755–759. [CrossRef] [PubMed]

44. Lee, J.-Y.; Talhi, O.; Jang, D.; Cerella, C.; Gaigneaux, A.; Kim, K.-W.; Lee, J.W.; Dicato, M.; Bachari, K.; Han, B.W.; et al. Cytostatic hydroxycoumarin OT52 induces ER/Golgi stress and STAT3 inhibition triggering non-canonical cell death and synergy with BH3 mimetics in lung cancer. *Cancer Lett.* **2018**, *416*, 94–108. [CrossRef] [PubMed]

45. Klosa, J. Synthesis of various cyanoacetic acid hydrazide derivatives. VII. Synthesis of tuberculostatic agents. *Arch. Pharm. Ber. Dtsch. Pharm. Ges.* **1955**, *288*, 452–455. [CrossRef] [PubMed]

46. Ottoni, O.; Cruz, R.; Alves, R. Efficient and simple methods for the introduction of the sulfonyl, acyl and alkyl protecting groups on the nitrogen of indole and its derivatives. *Tetrahedron* **1998**, *54*, 13915–13928. [CrossRef]

47. Cummings, D.F.; Canseco, D.C.; Sheth, P.; Johnson, J.E.; Schetz, J.A. Synthesis and structure–affinity relationships of novel small molecule natural product derivatives capable of discriminating between serotonin 5-HT1A, 5-HT2A, 5-HT2C receptor subtypes. *Bioorg. Med. Chem.* **2010**, *18*, 4783–4792. [CrossRef]

48. James, P.N.; Snyder, H.R.; Boekelheide, V.; Knowles, R.N. Indole-3-Aldehyde. *Org. Synth.* **2003**, *39*, 30. [CrossRef]

49. Kirsch, G.; Abdelwahab, A.B.; Hanna, A.G. Synthesis of Novel 3-Acetyl-2-aminothiophenes and Investigation of their Behaviour in the Reaction with Vilsmeier–Haack Reagent. *Synthesis* **2016**, *48*, 2881–2888. [CrossRef]

50. Tymiak, A.A.; Rinehart, K.L.; Bakus, G.J. Constituents of Morphologically Similar Sponges-Aplysina and Smenospongia Species. *Tetrahedron* **1985**, *41*, 1039–1047. [CrossRef]

51. Mazumder, A.; Lee, J.-Y.; Talhi, O.; Cerella, C.; Chateauvieux, S.; Gaigneaux, A.; Hong, C.R.; Kang, H.J.; Lee, Y.; Kim, K.-W.; et al. Hydroxycoumarin OT-55 kills CML cells alone or in synergy with imatinib or Synribo: Involvement of ER stress and DAMP release. *Cancer Lett.* **2018**, *438*, 197–218. [CrossRef] [PubMed]

52. Schnekenburger, M.; Grandjenette, C.; Ghelfi, J.; Karius, T.; Foliguet, B.; Dicato, M.; Diederich, M. Sustained exposure to the DNA demethylating agent, 2′-deoxy-5-azacytidine, leads to apoptotic cell death in chronic myeloid leukemia by promoting differentiation, senescence, and autophagy. *Biochem. Pharmacol.* **2011**, *81*, 364–378. [CrossRef] [PubMed]